POLITECNICO DI TORINO

Master's Degree Course in Electronic Engineering

Master's Degree Thesis

Development of a 3D printed Micro Free-Flow Electrophoresis Lab-On-A-Chip

Supervisors

Dr. Matteo Cocuzza

Dr. Simone Marasso

Candidate

Alessio Raiti

Student ID: 243899

Internship Tutor

Dr. Federica Barbaresco

Academic year 2019/2020

Table of contents

Abstract

This master thesis project is inserted within the DEFLeCT (Advanced platform for the early detection of not small cells lung cancer) project founded by Piedmont "Health & WellBeing" Platform in collaboration with Aizoon Consulting s.r.l., Politecnico di Torino, Università di Torino, Azienda Ospedaliera S. Luigi, Abich s.r.l., Chimete s.r.l., Essebi s.r.l., Fluody s.r.l., Gem Chimica s.r.l., Human Brain Wave s.r.l., Honestamp s.r.l., Lamp s.r.l., Osai S.p.A., Consorzio Proplast, Renishaw S.p.A., S.In.Co.S. Applications s.r.l., STV Italia s.r.l., Trustech s.r.l.

In the last few year, there has been an increase in the research of biological disease indicators called biomarkers. They are molecules or processes related to a specific disease. Significant organizations such as WHO (World Health Organization) have stated that these biomolecules can be useful to improve diagnosis and speed up the research of associated medical therapies.

This master's degree thesis is intended to produce an advanced platform for the early detection of non-small cells lung cancer (NSCLC). In particular, the project is focused on developing a microfluidic Lab-On-A-Chip capable to isolate exosomes biomarkers. Analyzing the literature, no example of μFFE (micro free flow electrophoresis) devices capable to do that can been found. Such chip manages to perform at a microscale level the free-flow electrophoresis that is indicated through its acronym μFFE.

The device is composed of a microfluidic separation chamber, some inlets in which sample and buffer solutions are pumped by using a pumping system, some outlets from which the separation

products are collected after the electrophoresis process. The chip was designed by using a commercial computer graphic CAD software called Rhinoceros and fabricated by employing a 3D printer (OBJET 30 provided by Stratasys) based on the poly-jet technology. Different design solutions were analyzed and some attention was dedicated to realize excellent standard fluidic connectors on the back of the chip. Firstly, a Luer slip standard connection was designed and its functionality was analyzed. Then, the design was improved by realizing threaded more robust connectors of kind UNF 28 standards. After the fabrication of different prototypes, a significant amount of time was spent to verify and compare the dimensions of the printed devices with the nominal values set on the CAD. In particular, measurements were collected and statistical analysis was carried out to compare the accuracy of the 3D printer in fabricating the device by the Matte and Glossy surface finished modes. In the second part of the work, the quality of the chip sealing was investigated and separation tests on a dye mixture composed by Bromophenol Blue and Xylene Cyanol FF were performed.

Acknowledgements

My university career has finished. Thus, I thank all my Professors of the DET since my technical knowledge has grown. My heartfelt thanks to the professor Matteo Cocuzza and his wonderful course, to the researcher Simone Marasso and a very huge thanks to the Phd student Federica Barbaresco. In addition, I thanks my parents for their support and I can't remember the day when they said to me that my idea to choose Politecnico was great because it is a very wonderful university. I dedicate my Master's Degree Thesis to my father with the aim of showing him that in our life never we must give up towards obstacles. A big thanks to Edoardo Mandalari, a friend of mine for the hours spent together, you have been a great friend from university and even thanks to Ioannis Stratakis, another university mate for the days spent in Politecnico with the purpose of studying. Finally, thanks to Stefano De Carlo, Federico Miranda, Giorgio Ducato, the Dr. Jeanpierre Francois and the future engineer Alessio Grillone, some friends of mine, who supported me during these years.
Thanks to all my laboratory mates!

Ever tried. Ever failed. No matter. Try Again. Fail again. Fail better.

(Samuel Beckett)

1.
Introduction

This chapter has the primary function to introduce the reader to the biomarker's research as a noninvasive investigation-technique also called liquid biopsy for the lung cancer [1]. Subsequently, the attention will be focused to describe the generic principle of electrophoresis, the free flow zone and its miniaturized microchip application which is defined through its acronym μFFE (micro free-flow electrophoresis). The existing devices and their applications will be deeply discussed, focusing on the fabrication technologies and materials.

1.1 The lung cancer biomarkers

Concerning the cancer, some associated biomarkers can be DNA, mRNA, proteins coming from the neoplastic cells. The exosomes are nano-sized vesicles that include the previous biological entities. The profiling of proteins contained by these nano-sized vesicles could help in speed up the NSLC (non-small lung cell) cancer diagnosis [2]. In the last few decades, some efforts have been spent researching high-performance separation methodologies capable of isolating such biological indicators since the existing separation techniques such as centrifugation are time-consuming [3]. In the broad set of techniques, the electrophoresis and in particular the free flow one shows excellent characteristics.

1.2 State of the art of μFFE devices

During the years, different ways to perform the electrophoresis have been exploited. In the wide set of techniques, the free flow electrophoresis has found success. In particular it has been implemented at a microscale level through μFFE (micro free-flow electrophoresis) devices. There are several advantages in passing at the micro-scale, such as the reduction of joule heating and the possibility to perform a chemical separation, by consuming a minimal amount of resources [4]. The heat issues are solved by employing a microchip thanks to the higher intrinsic heat dissipation proper of small devices. Such kind of electrophoresis technique consists of pumping a mixture that contains the analytes of interest through input section inside a microfluidic chamber and in collecting the separated and purified molecules at the outputs.

The μFFE is interesting because it has better performances with respect to other electrophoresis techniques such as the CE since it is faster and allows to carry on a continued separation inside a microfluidic volume without the need to reload the sample each time [5]. For this reason, it suits well to be employed in all applications in which a continuous purification process is fundamental (see Fig 1.1).

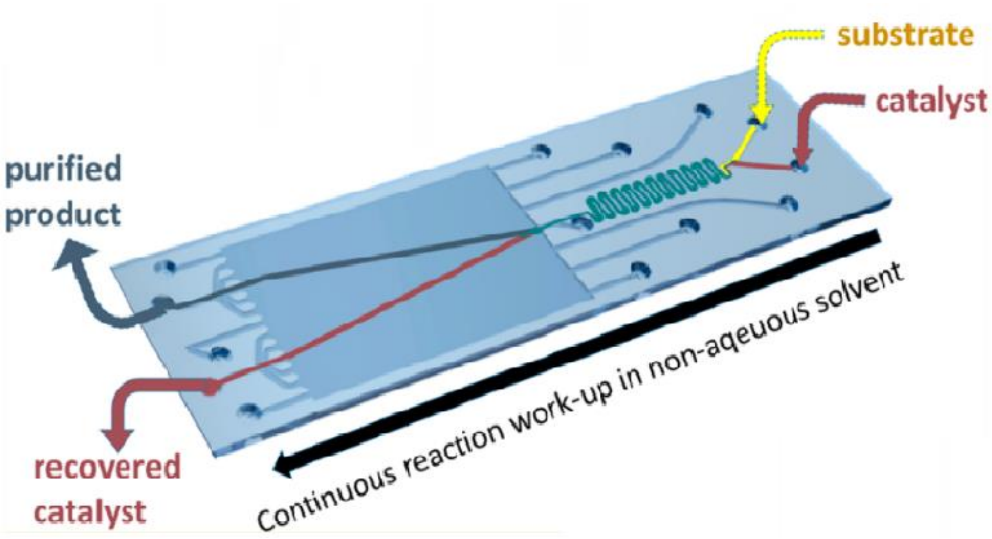

Fig. 1.1 – The figure shows a nonaqueous μFFE chip employed for realize a sample purification by means of catalyst introduction [17].

In particular, during the last few years, chemical Lab-On-A-chip has been employed in a vast variety of fields and in a miniaturized form. The μFFE has found success to be employed as a fundamental part of μTAS (miniaturized Total chemical Analysis System [6]. These modern devices implement a full laboratory in a tiny chip by automating and including all steps required by a chemical process, such as sampling, transport, filtration, dilution, elution, separation and detection, etc**.** By integrating the process entirely in a chip, there are many advantages and in particular, an efficient connection among each functional block can performed. Moreover, the μTAS has other vital benefits: low analyte diffusion, high sensitivity and speed up the biochemical reaction [7].

The micro free-flow electrophoresis chips have been employed with excellent results to analyze the mitochondria by wasting less time, sample, buffer and by applying lower voltages with respect to the well-known CE technique [8].

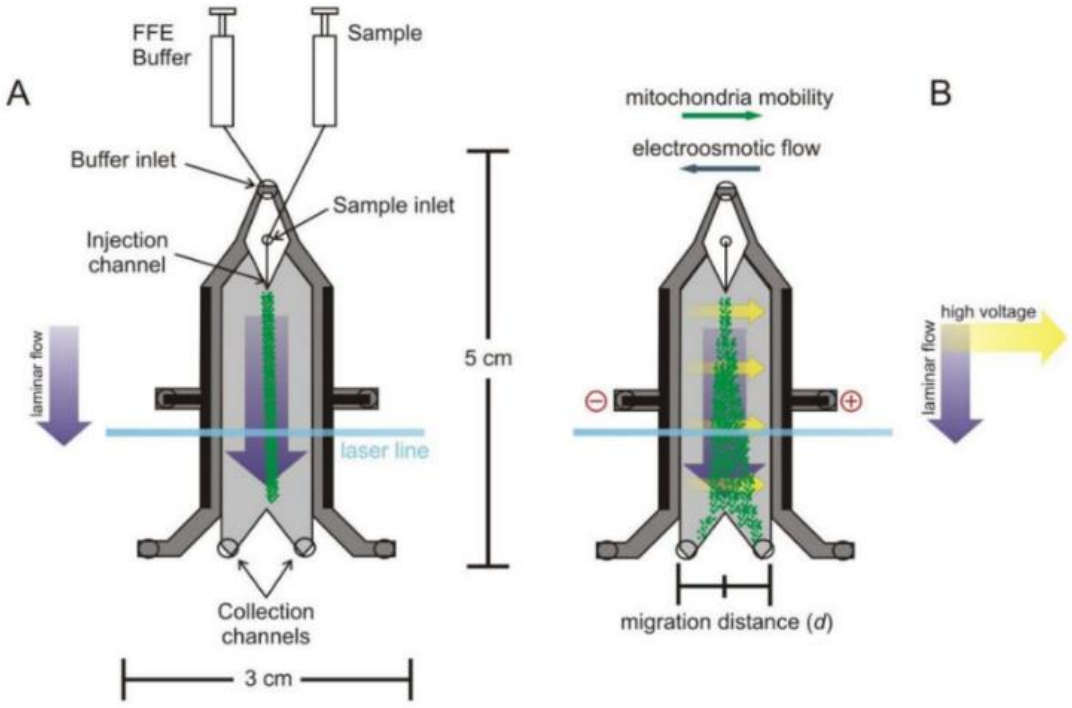

Fig. 1.2 – The figure shows a schematic of a μFFE device capable to separate the mitochondria [8].

The mitochondria are specialized organelles that can be found in eukaryotic cells. Their study is fundamental to analyze some pathological states because they regulate cell proliferation [8]. Another interesting application of the μFFE devices is their employment as online detection systems as pre-stage before performing analysis with mass spectrometry. The separation and sorting of substances are fundamental to have a precise diagnosis or to prepare a purified sample. The identification of biomolecules such as AMP, ATP and CoA has been demonstrated using a μFFE chip in couples with a mass spectrometer [9]. Another field in which this technique can be successfully employed is aerospace technology thanks to its easy implementation, which requires the consumption of small resources [10]. In recent years, space life science research has become an independent branch. As a result, the study of the biological effects of the cosmic environment on human tissue has become fundamental to understand the possible issues. Some chips have been fabricated for aerospace research to propose devices with reduced undesired effects, such as low Joule heating, demonstrating great separation performances in harsh environments such as the cosmic one. Another fundamental task needed at the microscale level is the performance of a continuous separation process for monitoring a specific substance concentration with respect to some unhealthy levels. The μFFE shown excellent results in conducting contaminants research in significant fields such as food safety [11]. In the last decades, strict rules have been formulated to monitor the contamination of pesticides and veterinary drugs. In this regard, particular ssDNA and RNA sequences called aptamers are used to bind with high affinity to specific target dangerous molecules. It has been demonstrated that aptamers can be isolated by using the micro free-flow electrophoresis. Such chips can be part of a Lab-On-A-Chip, which implements the SELEX process in a miniaturized form [11]. It replaces the separation step, usually performed by CE with which only few nanoliter of solution can be processed without losing the separation resolution or CMACS (Continuous Magnetic Activated Separation), which requires a vast amount of time to be performed. In pathological diagnostics, it is often necessary to improve the detection sensitivity for specific analytes (molecules, biomarkers). For such reason, a preconcentration step is usually required to conduct functional analysis.

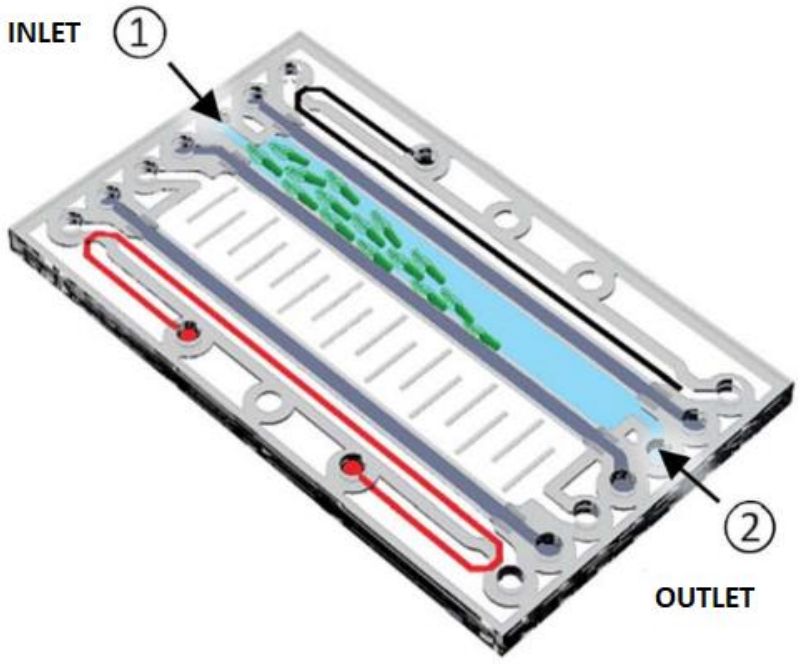

Fig. 1.3 – Lab-On-A-Chip employed to concentrate bacteria by means of a free flow electrophoresis process and to realize a lysis process for the release of their genetic materials [13].

The most commonly used technique to perform this task is based on centrifugation, which spends much time, employs expensive machines and requires operator handling [12].
Thus, by implementing this process at a microfluidic scale, it is possible to automatize it. For instance, a sample of water can be contaminated with bacteria that are diluted in low concentration and not detectable. In such a kind of problem, the μFFE can be successfully employed as a pre-concentrator (see Fig. 1.3) before performing further detection steps such as nucleic acid amplification technique (NAT) that is used to distinguish certain kinds of pathogens [13].
Focusing now on some characteristics of the μFFE. The main problem of the chips is the bubbles generated by electrolysis [14]. Indeed, they can perturb the separation process and distort the flow profile inside the chamber. There are several techniques to isolate the electrode channels from the separation chamber. A widespread technique is the employment of a membrane but it requires an expensive fabrication process. In particular, the membrane can be tuned according to the needs by performing a chemical reaction of it with some chemical groups increasing in

such a way the performances and the selectivity. A common technique consists in the employment of isolated hydrogel membranes, which are used as separators thanks to their permeability to ions and the high hydrodynamic resistance [15]. In literature, some separation membranes are fabricated by using different materials. In particular, the PDMS, which has very high gas permeability, has been employed. Moreover, cellulose membranes can be fabricated and employed [16]

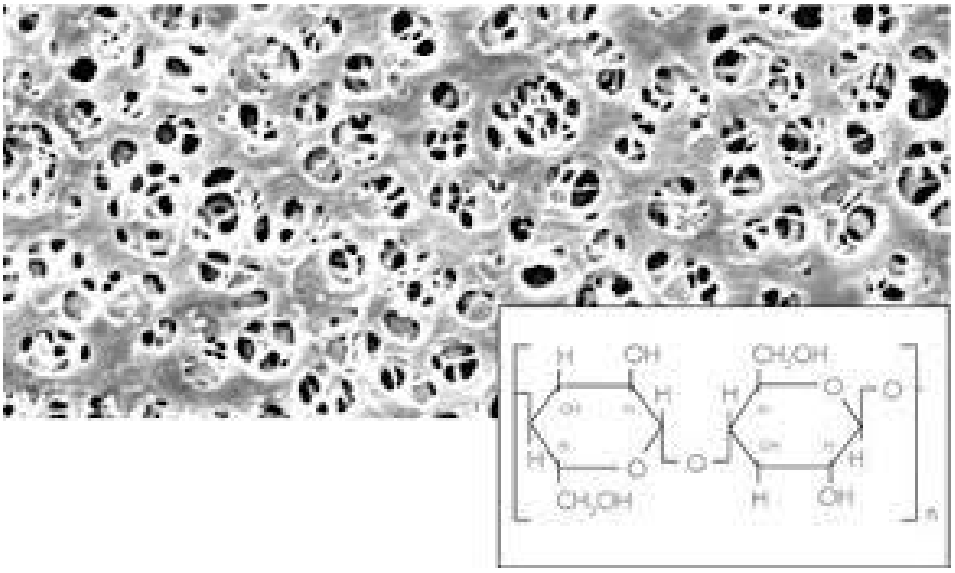

Fig. 1.4 – The figure shows a cellulose membrane employable in the μFFE devices to block the electrolysis bubbles.

Another hydrogel material that can be employed as a separator is PEG-DA [17][18]. It can be polymerized inside the chip by using a photopolymer made of a mixture of 40% water, 60% (w/w) PEG-DA and 1% (w/w) DMPA. Its employment is useful due to its excellent biocompatibility with the cells. Other materials, commonly employed for the fabrication are the acrylamide, the polycarbonate and the tetra-PEG gel. The main drawback of employing the previous membranes is their intrinsic electrical resistance, which reduces the voltage applied to the chamber by degrading in this way the chip performances. A different and modern approach to block the electrolysis bubbles is the design of partitioning bars (see Fig 1.5) that play the role of physical separators between the chamber and electrodes [19].

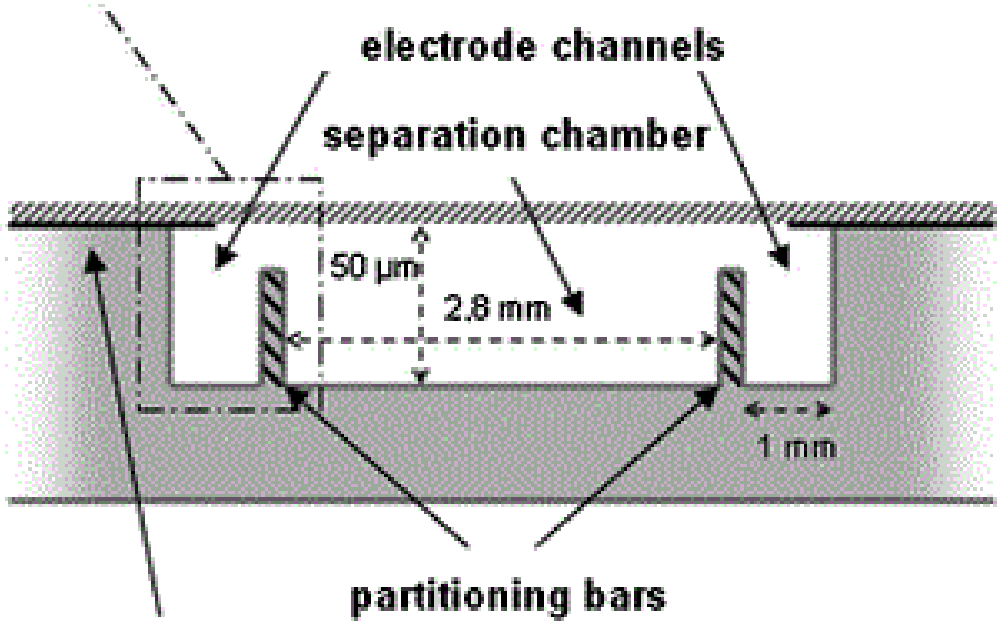

Fig. 1.5 – Schematic representation of a µFFE chamber with partitioning bars employed to separate the microfluidic chamber from the electrode channels.

Another approach in order to avoid the bubbles invasion consists of the reduction of the separation chamber sizes as much as possible. However, this technique can limit the throughput of the process too much by reducing the sample volume.

1.2.1 Materials and fabrication

In the last three decades, different materials with different properties have been considered for the fabrication of microfluidic devices. Indeed, the fabrication material's choice plays a fundamental role because the complexity of the technological process depends on it. The first materials which were employed are silicon and glass. In particular, the first real µFFE devices have been fabricated during the 90s by using silicon [20][29]. One of the reasons for this choice

stays in the improvement of the process integration. The fabrication with this material permitted an easy and direct integration with μTAS (micro Total Analysis System), which was patterned on a silicon wafer by using the most common micromachining techniques.

The silicon is a semiconductor material usually employed in microdevice fabrication. It shows some characteristics: one of the greatest is its high organic solvents resistance, which allows to clean the chip by using some solution such as the acetone without damaging the surfaces. Other advantages of this material are the natural metal deposition, the stable electroosmotic mobility, the vertical sidewall [30] and the possibility to build high aspect ratio structures (usually up to 20:1). However, in the recent years, it has become an unattractive material and it has been replaced by other solutions since it is too hard and requires too expensive and dangerous processes. In particular, its patterning requires etching processes performed by using dangerous acids. Moreover, the bonding of two pieces of such material requires a very high temperature, pressure and it needs to be performed in a cleaning room to avoid surface contaminations. One of the main limitations of the silicon is its opacity in the visible range. Therefore, in this case, it is impossible to monitor an electrophoretic process by looking inside the separation chamber in real-time. Another big drawback of silicon is the low breakdown voltage, which limits drastically the separation power of a μFFE chip. Focusing on the broad set of available materials employable for the μFFE fabrication, the glass stands out. This material has the great advantages of being compatible with a biological sample and having low surface absorption.[30] It is a hard material which requires high temperatures and pressures to perform an optimal bonding procedure. Other significant intrinsic advantages are the good breakdown voltage and the optical transparency in the visible range which makes this material more attractive with respect to silicon. During the last few years, several devices have been fabricated by using glass and borosilicate glass [10][11][13][17][18].

Fig. 1.6 - μFFE device fabricated by using a glass wafer [41].

However, nowadays, new classes of material are considered for microfluidic device fabrication. In particular, the polymers are becoming excellent candidates for such purpose.

Focusing on the full range of available materials, the PDMS surely is the most popular one thanks to its great features. Indeed, it is cheap and it suits well to apply the moulding technique. However, it is quite permeable to gases [32]. This characteristic creates problems in hindering the electrolysis bubbles generated into the electrode channels. Moreover, this elastomer shows non-specific adsorption issues and as a consequence, it needs a specific treatment to be employed for the μFFE chip fabrication. During the years, some devices have been realized by using this material [19][22]. Focusing on the thermoplastic group, the PMMA (Poly (methyl methacrylate)) and the ABS (Acrylonitrile butadiene styrene) are usually employed. These materials are clear optically, no permeable to gases. Moreover, they can be easily patterned through

a moulding technique allowing in such a way the rapid prototyping and mass production. Moreover, the PMMA is cheap and compatible with the electrophoresis process. Recently, a new class of polymer called COC (cyclic olefin copolymer) aroused researchers' attention thanks to their excellent properties, such as easy fabrication, optical transparency, biocompatibility and chemical resistance [33]. However, these materials have adsorption problems that require surface treatments in order to reduce undesired effects.
Considering the fabrication by employing such material, the microfluidic net is patterned using the micromachining with CO2 laser, hot embossing and injection moulding. Moreover, bonding techniques such as microwave bonding, thermal fusion bonding and adhesive bonding can be exploited to seal the device [30].

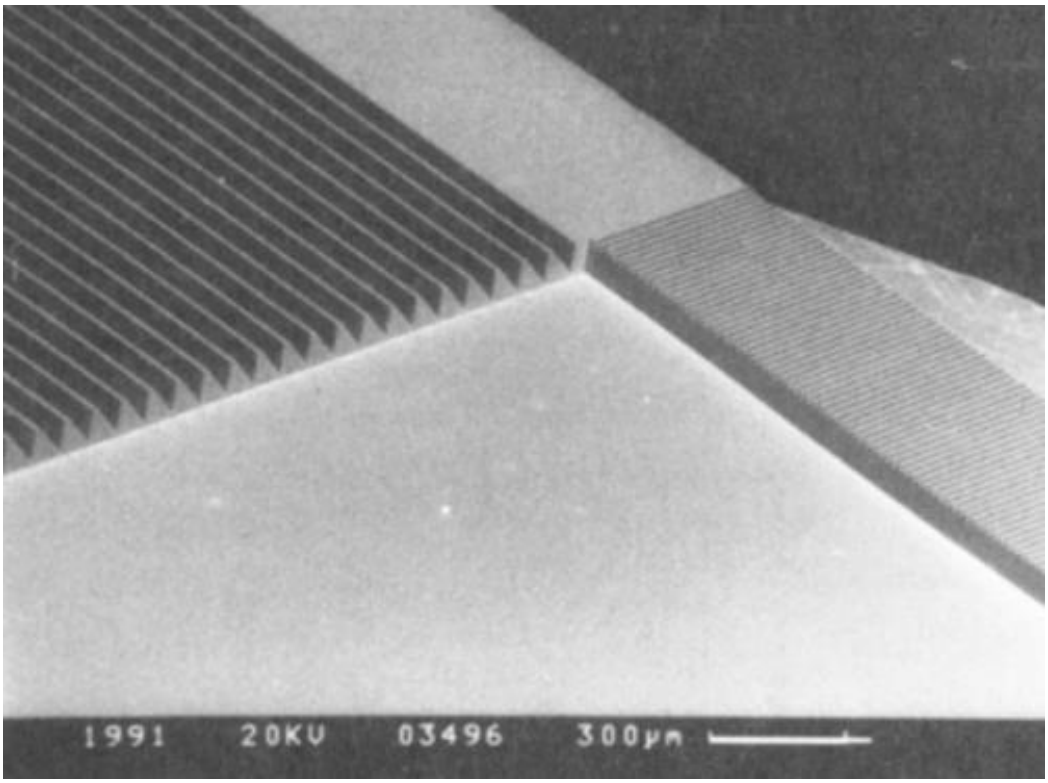

Fig. 1.7 – FESEM image of the inlet channel array of a microfabricated µFFE [20].

As already mentioned, the first employed materials have been silicon and glass. In particular, for the first one, the device fabrication starts from a silicon wafer n-type doped ($10^{15}/cm^3$) [20]. For

the second material, the chip is fabricated starting from a Pyrex glass one. In particular, the fabrication recipes are similar in both cases. Microfluidic geometry, etchants and the electrodes' material can change among the different fabrication processes, but the flow is similar for such fabricated devices. The silicon and glass are patterned by using micromachining techniques (see Fig 1.7) that require expensive processes and machines. The three most commonly employed techniques to pattern these substrates are: surface micromachining, buried channel technique and bulk micromachining (see Fig 1.8). In the first technique, a sacrificial layer (usually the silicon dioxide) is employed to design the desired microfluidic chamber and channels onto the substrate. The thickness of the sacrificial layer can be controlled during deposition with a precision of few nanometers [21].

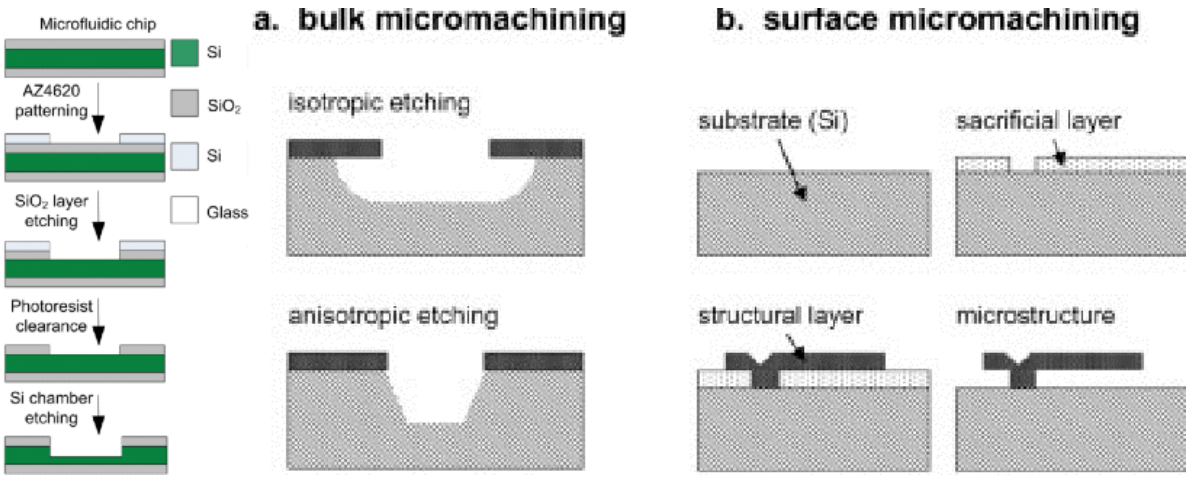

Fig 1.8 – Surface and bulk micromachining.

After the micromachining, sandblasting, drilling, or laser drilling can be employed to create the device inlets and outlets. As already mentioned, another important fabrication technique that is largely employed to fabricate the microfluidic devices is the microinjection moulding (see Fig 1.9).

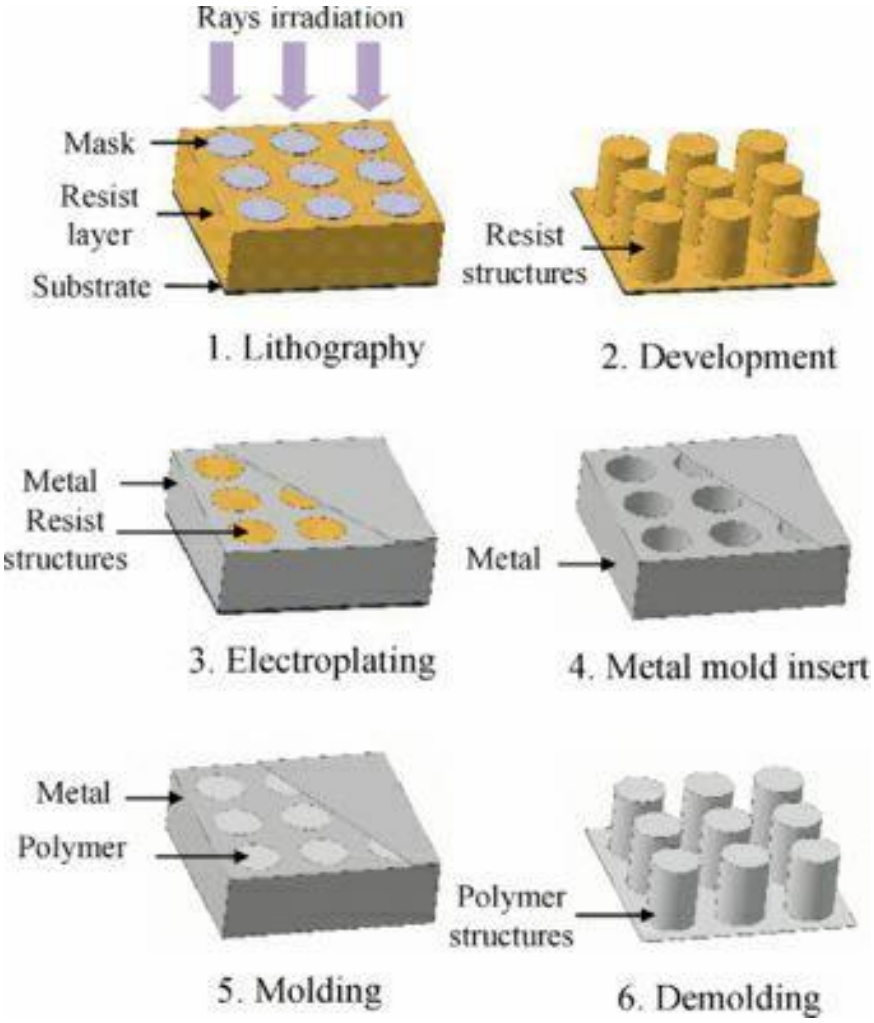

Fig. 1.9 –The figure shows the steps to fabricate a master mold and the microinjection moulding

Nowadays, it is becoming popular to be used for the rapid production of cheap polymeric devices. The μFFE fabrication by using such technique have been performed by Xiaotong Fu [22]. In particular, the entire device has been fabricated by injecting a carbon-nano powder and PDMS mix into the mould. The electrodes have been fabricated in gallium. A significant advantage of such fabrication technique is that it can be automatized with a wide range of polymeric materials [23]. In this process, a thermoplastic molten material is injected into a mold cavity and it is compressed (see Fig 1.9). When the temperature decreases, the material becomes solid and it keeps the needed mold shape. The process is based on the fabrication of a master mold, which can be realized by using SU-8 photoresist and by employing conventional techniques such as spin coating [24].

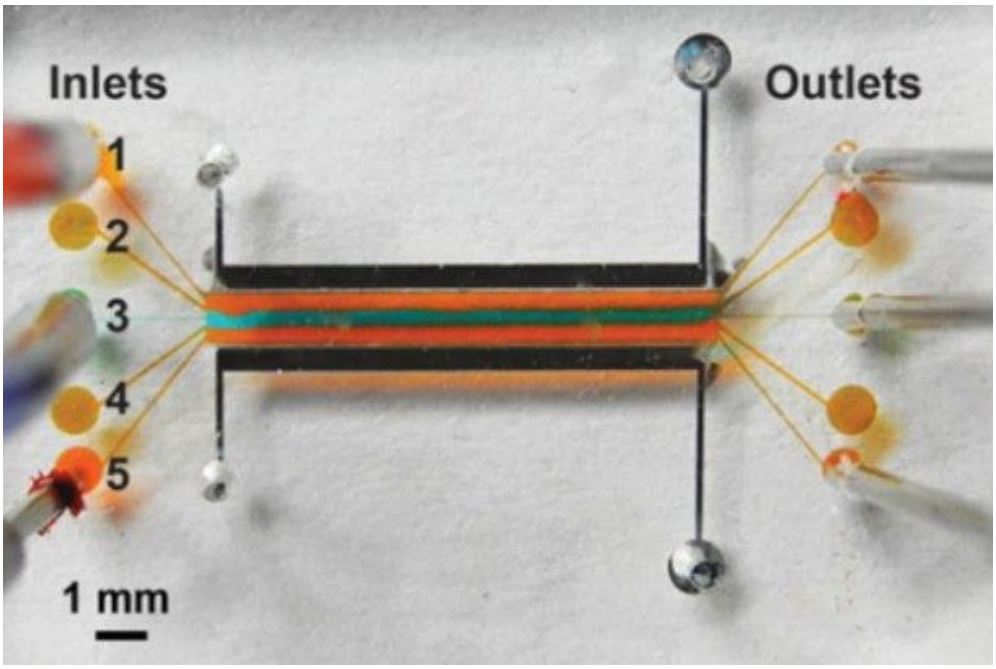

Fig. 1.10 – μFFE device fabricated by using the microinjection molding and the PDMS material [22].

After the microfluidic design and the implementation of the previous fabrication processes, the chamber of the device must be sealed in order to avoid contaminations.

Fig. 1.11 – The picture shows the sealed chamber of a μFFE device realized in glass [6]

This fabrication step is performed by using some common techniques such as thermal, anodic (see Fig 1.12) or adhesive bonding in order to seal the device with a lid. The first technique can be used to seal a chip by performing for instance a glass to glass (see Fig 1.11) or silicon to silicon bonding [25]. It consists of clamping together two perfectly cleaned glass substrates fabricated previously and sealing by using heat. The technique is slow and it needs the use of a furnace with a temperature regulator.

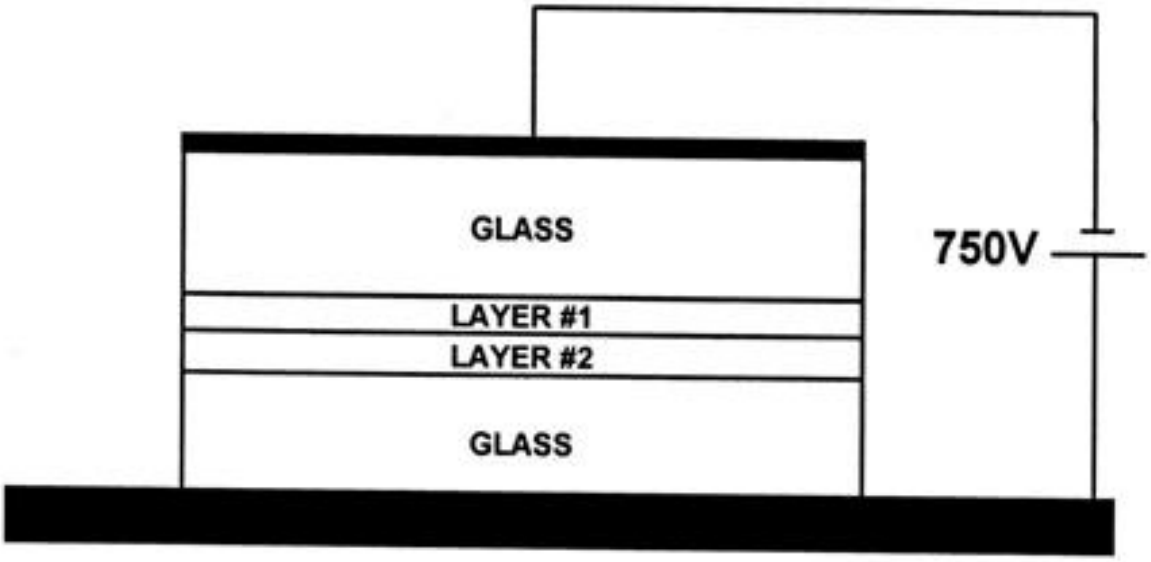

Fig. 1.12 – Anodic bonding representation [26].

The second bonding technique has some advantages such as simplicity and moderated implementation costs. The process consists of pressing together two substrates with selected layers between and it consists in applying heat and voltage for a certain period of time [25]. During such process, all pieces must be cleaned and kept perfectly in contact. Another technique for seal the μFFE is the adhesive bonding (see Fig 1.13). It is a widespread technique which consists in applying an adhesive layer among two surfaces. Then, the bond can be performed thanks to evaporation of a solvent, heat curing or UV curing [26]. The main advantage of this technique is the ease of implementation. It is important for this process to distribute the resin solution with uniform consistency and to select the proper solvent.

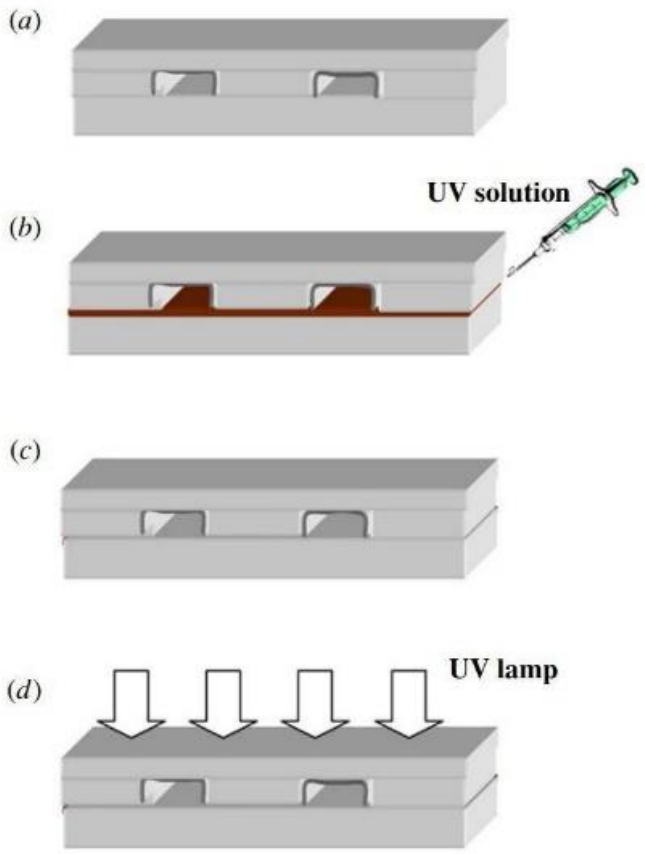

Fig. 1.13 – Fabrication steps to perform an adhesive bonding.

Focusing now on the electrical parts of the micro free- flow electrophoresis devices. The electric field used for the molecular separation is applied to the separation chamber by employing two electrodes which lie on two appropriate channels where the electrolysis process takes place. The electrodes have the shape of a strip or a wire. They are usually inserted into the device manually, or they are built during the whole chip fabrication by using some processes [27]. The material for the fabrication of the electrodes must have as low resistivity as possible. In particular, the voltage drop must be as low as possible for not degrade the device performances. It is the reason why the most commonly employed materials are metals such as platinum, copper and gold. The electrodes can be fabricated by performing a sputtering process [18]. This technique is a deposition method employed to create a thin film (see Fig 1.14). The material is ejected from a source and it is directed to the target substrate. The advantage of this method consists in the possibility

to deposit also materials which have a high melting point. Indeed, it suits well to deposit Au and Ti films [28].

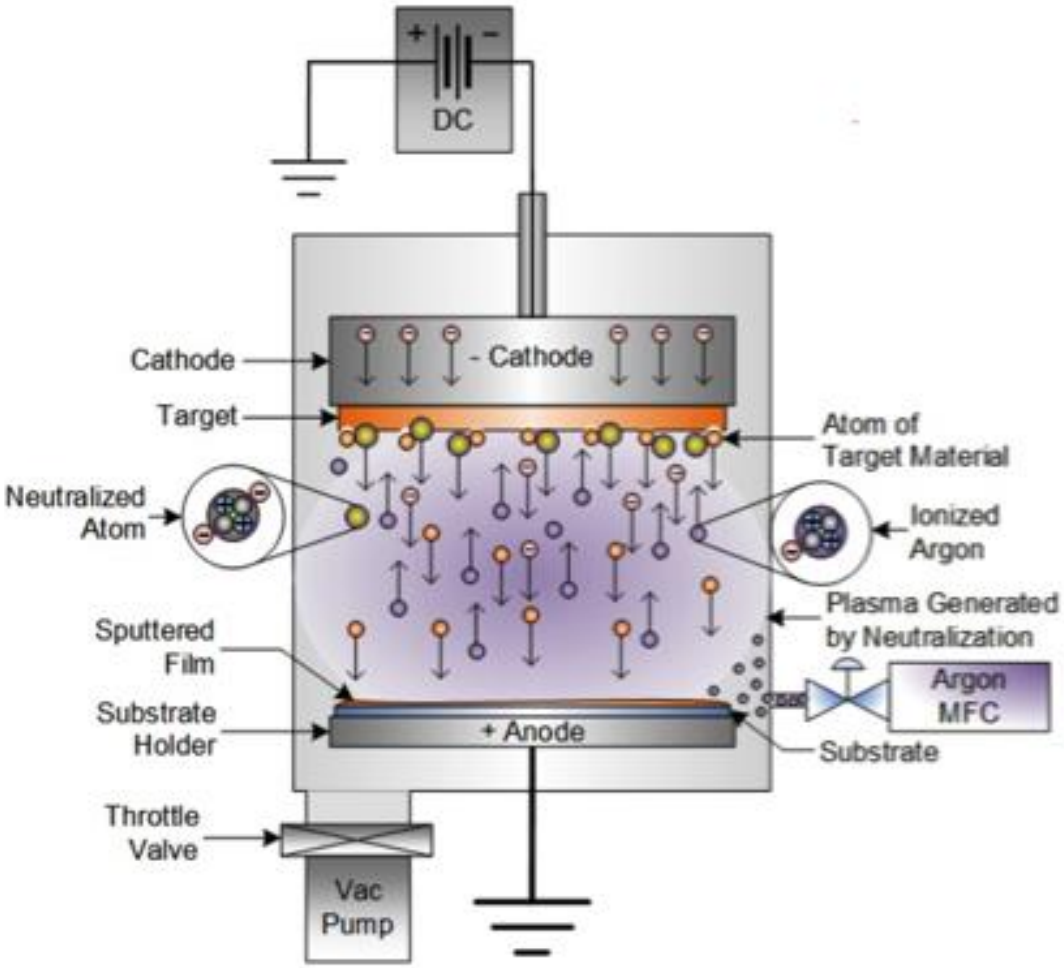

Fig. 1.14 - Plasma enhanced sputtering reactor.

After the deposition, in order to pattern properly the two metals, a standard photolithography process has to be performed. Subsequently, a silver conductive epoxy bonding can be performed to connect the external wires. However, before to perform the previous deposition techniques, a good workaround that prevents the current flow into the substrate and creates damages is the deposition of an insulating layer onto the silicon for increases the breakdown voltage.

1.3 The principle of electrophoresis

The electrophoresis is an electro-kinetic phenomenon employed mainly in biology, biochemistry and medicine as a high-resolution investigation and analytical technique. It is based on the separation of electrically charged particles, molecules, colloids submerged in a stationary fluid, usually an aqueous buffer solution. The employment of this last mixture is necessary to perform the electrophoresis process correctly since this fluid rich of ions transfers the electrical charge allowing in such a way to achieve the separation. Besides, it manages to keep steady the pH gradient inside the separation chamber that is fundamental to perform the zone electrophoresis [34]. The buffer must be chosen according to the sample solution and to the nature of the analytes. For instance, the use of a zwitterionic organic chemical substance called HEPES (N-2-Hydroxyethylpiperazine-N'-2-Ethanesulfonic acid), diluted in the proper concentration, suits well to perform the electrophoresis in biological tissues and blood [35]. Two significant advantages in employing this technique are that it does not perturb the molecules' structures and it has high sensitivity in distinguishing the differences in charge and size of particles and molecules [36]. The phenomenon is based on the application of an electric field employing an anode and a cathode. In particular, it is applied in the volume which contains the sample solution. Then, after a certain amount of time under the force of the applied electric field, the particles start to migrate with different speeds, according to their surface charge and mass, towards the electrode, which has the opposite sign.

The movement of positive ions toward the negatively charged electrode is called "Cataphoresis" while the flow of negative ions toward the positively charged electrode takes the name of "Anaphoresis." During the last decades, this separation technique has been successfully employed to isolate a wide variety of substances such as DNA, proteins, peptides, amino acids, drugs [36]. There are different modes to perform electrophoresis: isoelectric focusing, isotachophoresis and zone electrophoresis [36]. They are based on different principles and they have found success in the separation of different molecules. An essential mode is the isoelectric one. This technique allows us to separate some proteins according to their net charge. In particular, the isoelectric

point of a specific protein is the pH value for which it shows a charge equal to zero. This technique is performed by placing the sample containing the analytes in a pH gradient slab generated by an electric field [36]. After a certain amount of time, the proteins start to migrate through the pH gradient under the force provided by the applied electric field, until they reach their isoelectric points. Subsequently, the separated substances are collected in proper zones or bands. Another common technique is the isotachophoresis. This technique is used to separate ionic substances. In particular, it is based on the difference between analytes electrophoretic mobility. The process involves two different electrolytes called leading and terminating [37]. To perform such separation technique, the analytes' mobilities must satisfy the following equation:

$$\mu_L > \mu_A > \mu_B > \mu_T \tag{1.1}$$

Nowadays, the different electrophoresis techniques have been implemented in the form of a microchip by allowing in such a way to perform an ultra-fast separation, to improve the resolution thanks to the reduction of some undesired effects and to improve the fabrication process by reducing costs. In particular, the researchers are dedicating efforts to developing automated ways to perform chemical large-scale analysis in a microchip, by fabricating and employing tiny devices called Lab-On-a-Chip.

1.3.1 The zone electrophoresis

In this kind of electrophoretic mode, the charged ions and particles migrate towards the electrodes with an opposite charge, under the force, supplied by an applied electric field [36]. When the separation occurs, different flows and zones are created and they draw away from each other by becoming independent. The main drawback during the performance of such a process is the diffusions of the analytes. Therefore, the process must be performed in a proper support medium, which can be a gel or a filter paper to obtain the right flows. After the separation, the different products are collected in different zones. Focusing now on two common examples of such electrophoresis performed by using the agarose and the polyacrylamide gels. The PAGE

(polyacrylamide gel electrophoresis) is commonly employed to divide proteins (see Fig 1.15). There are two kinds of it: the dissociating and non-dissociating [36]. The first one allows us to separate the proteins conserving their structures, functions and activities.
Therefore, this procedure can be useful to isolate proteins employed in subsequent experiments.

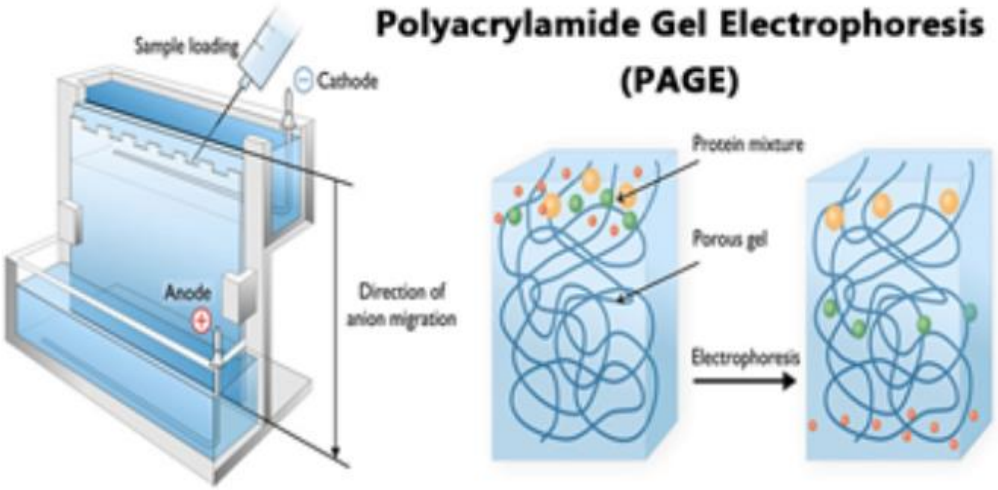

Fig. 1.15 – The figure represents a way to perform an electrophoresis process by mean of the Polyacrylamide gel. The sample is a proteins mixture. After the separation, they are collected in different zones of the gel matrix.

On the contrary a dissociating gel is employed to divide the proteins into its constituent polypeptides which can be analyzed. Another common electrophoresis technique is based on the Agarose gel (see Fig 1.16). Such technique is performed by employing this polysaccharide which is constituted by some pores with a diameter in the range from 100 to 300 nm [36]. In particular, the gel concentration is related to the sizes of them. This separation technique, is commonly used to perform the zone electrophoresis to divide DNA and RNA segments.

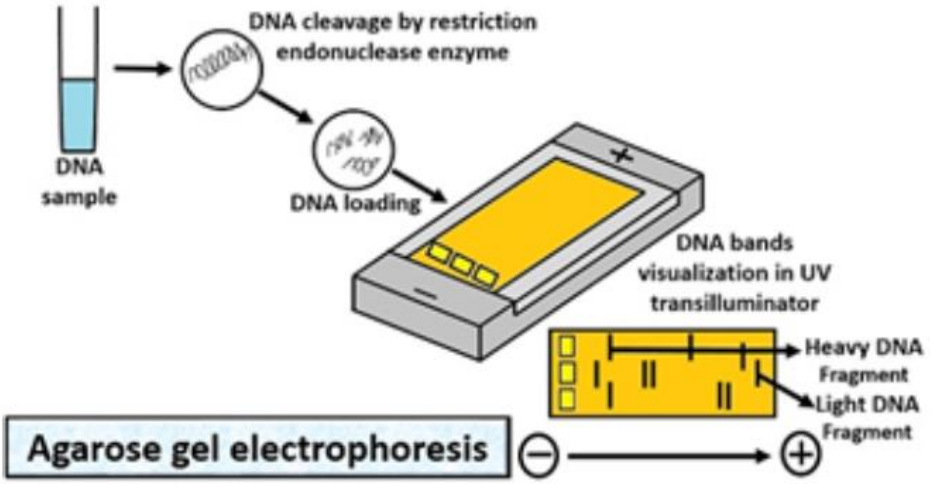

Fig. 1.16 – In this picture, some DNA fragments is obtained performing the electrophoresis by employing an Agarose gel matrix.

Another widely employed technique to perform the electrophoresis is the capillary one (see Fig 1.17). It used in genetic analysis, drug discovery and protein characterization. It is carried out in thin capillary glass, quartz, or plastic tubes with an inner diameter of about 1 to 10 Â. The buffer solutions employed in this electrophoresis are usually the SDS-PAGE for proteins separation or TAE in the other cases [36]. These solutions are pumped inside the pipes. The time employed to perform the capillary electrophoresis is quite short.

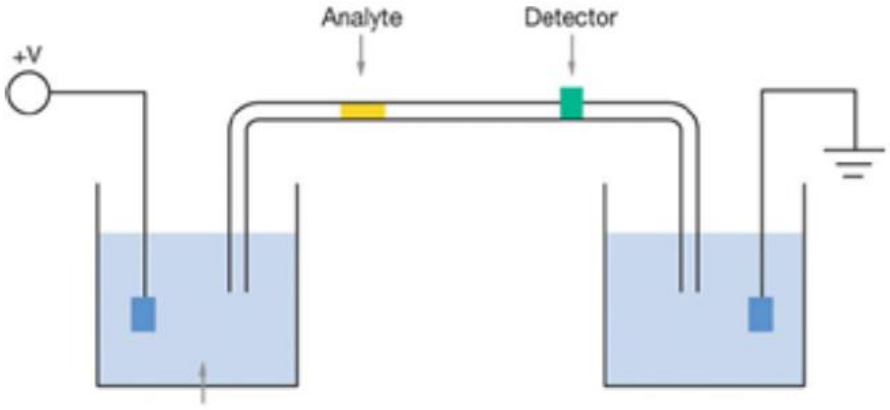

Fig. 1.17 – Schematic representation of the equipment used to perform the capillary electrophoresis.

1.3.1.1 The micro free flow electrophoresis

The free flow electrophoresis is high resolution separation technique in which the electric field is applied perpendicular to a provided separation chamber (see Fig 1.18). The devices which implements such technique are filled with a mixture which contains the analytes that must be separated [6]. In particular a fluidic sample is pumped continuously inside the device through the sample introduction zone (see Fig 1.18).

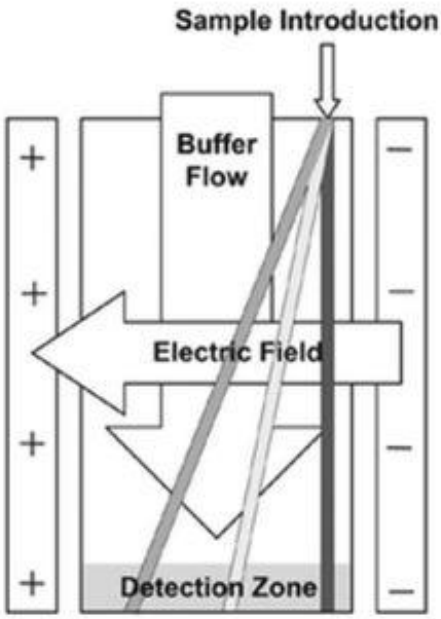

Fig. 1.18 – Schematic representation
of a microfluidic free flow electrophoresis chamber [6].

There are different ways to perform the free flow electrophoresis such as free-flow zone electrophoresis (FFZE), free-flow IEF (FFIEF), free-flow ITP (FFITP), and free-flow field step electrophoresis (FFFSE) [38].

In the set of techniques, the μFFE which belong to the FFZE is interesting. The micro free flow electrophoresis has some advantages with respect to the large-scale technique. The main advantage in passing to microscale is that the involved flows pass from a turbulent to a laminar regime. One of the main advantages of this technique with respect to employ other kinds of electrophoresis is the very high sample recovery rate. Indeed, the analytes must not adhere to a

gel matrix. Moreover, another benefit of the μFFE is the high separation resolution [6]. The main functional part of the μFFE devices consists on a precisely manufactured chamber fabricated usually by using two thin plates. The chips integrate some special channels which contain the electrodes which are placed in different orientations with respect to the chamber. These chip areas are used to provide the electric field required to perform a correct separation. In such kind of electrophoresis, the sample is infused into a thin laminar layer constituted in general by one or more separation buffers flows (see Fig 1.18) which move through the chamber with a certain speed. Then, the analytes exposed to the applied electric field are deflected in the lateral direction according to their electrophoretic mobilities [6].

1.4 Mathematical model in a free flow zone electrophoresis chamber

The separation chamber is provided by a proper coordinate system (see Fig 1.19). In particular the origin of the spatial axis is fixed in line with the point where the samples are injected.

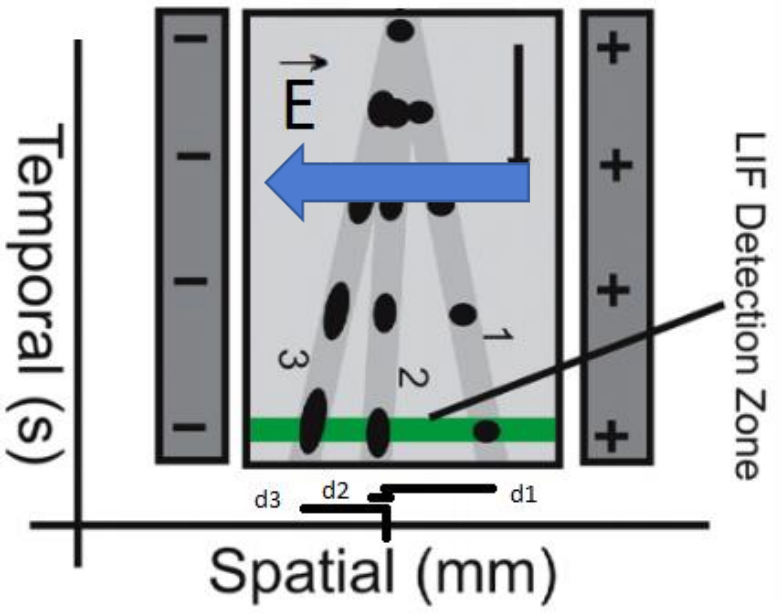

Fig. 1.19 – Micro free flow electrophoresis chamber with deflected analytes [31].

The deflection distance for a certain analyte is expressed as:

$$d = \mu_e E t \tag{1.2}$$

This distance represents the lateral migration into the μFFE chamber with respect to the origin. The particles are approximated as a sphere with uniform distributed charge on their surface. The μ_e represents the electrophoretic mobility of them and it is expressed as:

$$\mu_e = \frac{q}{6\pi r} \tag{1.3}$$

Where r is the ionic radius, η the viscosity. The injected sample is subjected to an electric field for a certain amount of time t which can be modified by changing the speed of the flows. Moreover, the electric field and the buffer flow velocities can be changed to optimize the FFE process independently. The flows of the analytes are not ideal streamlines but they are affected by a broadening effect which is described by means of an overall peak variance σ^2_{FFE} [6].

$$\sigma^2_{FFE} = \sigma^2_{inj} + \sigma^2_D + \sigma^2_{ED} + \sigma^2_{HD} + \sigma^2_{EHD} \tag{1.4}$$

The contribute σ^2_{inj} represent the injection stream.

$$\sigma^2_{inj} = \frac{w^2_{inj}}{12} \tag{1.5}$$

The term w^2_{inj} is the baseline width of the injection stream. Considering σ^2_D, it is the variance contribution due to the diffusion of the analyte inside the chamber.

$$\sigma_D^2 = 2Dt \tag{1.6}$$

The D indicates the diffusion function which is proper of the analyte while t indicates the transit time spent into the chamber. Another term which contributes to the overall variance is σ^2_{ED} which represents the effect of the electrodynamic broadening. This term can be found into devices where the electrodes are separated from the separation chamber [6]. The contribute σ^2_{HD} represents the effect of the hydrodynamic broadening and it is a contribution that is due to the difference in the profiles of the buffer flow which act on analyte in the longitudinal direction and the electric field direction of application which moves it laterally. This term cause, the analytes close to the chamber walls to move slower. Indeed, they spend more time in the electric field with respect to the one which is in the center of the chamber:

$$\sigma_{HD}^2 = \frac{h^2 d^2 v}{105DL} \tag{1.7}$$

h represents the height of the channel, d the deflection distance, v the buffer linear speed, D the diffusion constant and L the length of the separation chamber. If there is no separation barrier between the chamber and the electrode channels, the electrodynamic broadening can be neglected. The overall peak variance with some approximation, is expressed as:

$$\sigma_{FFE}^2 = \sigma_{inj}^2 + \sigma_D^2 + \sigma_{HD}^2 \tag{1.8}$$

By substituting, the single contributions the variance becomes:

$$\sigma_{FFE}^2 = \frac{w_{inj}^2}{12} + 2Dt + \frac{h^2 d^2 v}{105DL} \tag{1.9}$$

Considering the separation of a mixture composed by two analytes affected by the broadening effect but in which the EHD and ED contribution can be neglected. The resolution of the μFFE chip is expressed as follows:

$$R_S = 2\frac{d_1 - d_2}{w_1 + w_2} \tag{1.10}$$

By substituting the expression of the variance terms, the final expression of the resolution becomes:

$$R_S = \frac{(\mu_{tot1} - \mu_{tot2})Et}{2\left(\sqrt{\frac{w_{inj}^2}{12} + \frac{2D_1L}{v} + \frac{h^2 d_1 v}{105 D_1 L}} + \sqrt{\frac{w_{inj}^2}{12} + \frac{2D_2L}{v} + \frac{h^2 d_2 v}{105 D_2 L}}\right)} \tag{1.11}$$

By increasing the applied voltage, by increasing the transit time t or by increasing the electrophoretic mobility difference, the chip resolution improves. Moreover, by increasing the diffusion constants, the resolution decreases, by changing the chamber height h and length L the diffusion and the hydrodynamic broadening terms increase. Focusing the attention to the free flow electrophoresis of two common employed dyes: the Rhodamine 110 and the Rhodamine 123. The performances in term of separation resolution can be modified by changing the product Et and the buffer speed.

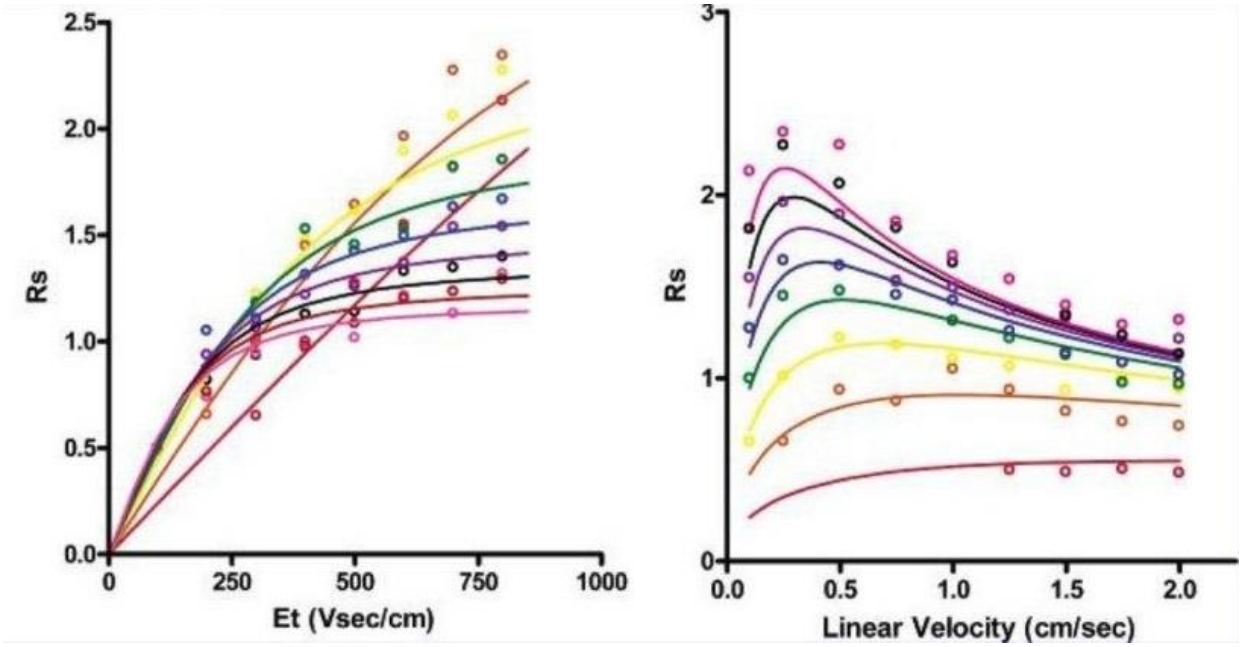

Fig. 1.20 – Variation of detection resolution for Rhodamine 100 and Rhodamine 123 separation as a function of the Et product and of the sample flow rate [16].

In high buffer speed regime, the resolution expression is simplified and it can be expressed in the following simpler form:

$$R_S \approx \frac{\Delta\mu}{4h\mu}\sqrt{\frac{105L}{v}} \tag{1.12}$$

This expression is interesting since if the buffer flow is too high, the resolution becomes independent from the applied voltage.

1.5 The surface adsorption

The adsorption in the substrate surface is a serious problem, especially for the molecules which are adsorbed irreversibly. Indeed, in such cases, extensive flushing and cleaning of the device are required. However, the surface adsorption can be reduced by applying a coating layer or modi-

fying the buffer by adding certain substances [39]. Considering the separation of the dyes described previously, the Rhodamine 123 is significantly adsorbed on the surface if the μFFE chip is fabricated by employing a glass substrate. Focusing on the electrophoresis of proteins, they create problems and are adsorbed onto solid surfaces of many materials. In particular, the adsorption is related to the surface charge of the substrate and the characteristics of the involved proteins [40] [41].

1.6 The temporal broadening

The temporal broadening is a phenomenon present in the μFFE devices. It consists of the change of the analyte distribution in width and peak as a function of time (see Fig 1.21). As previously cited, this effect is due to the surface adsorption of the substrate.

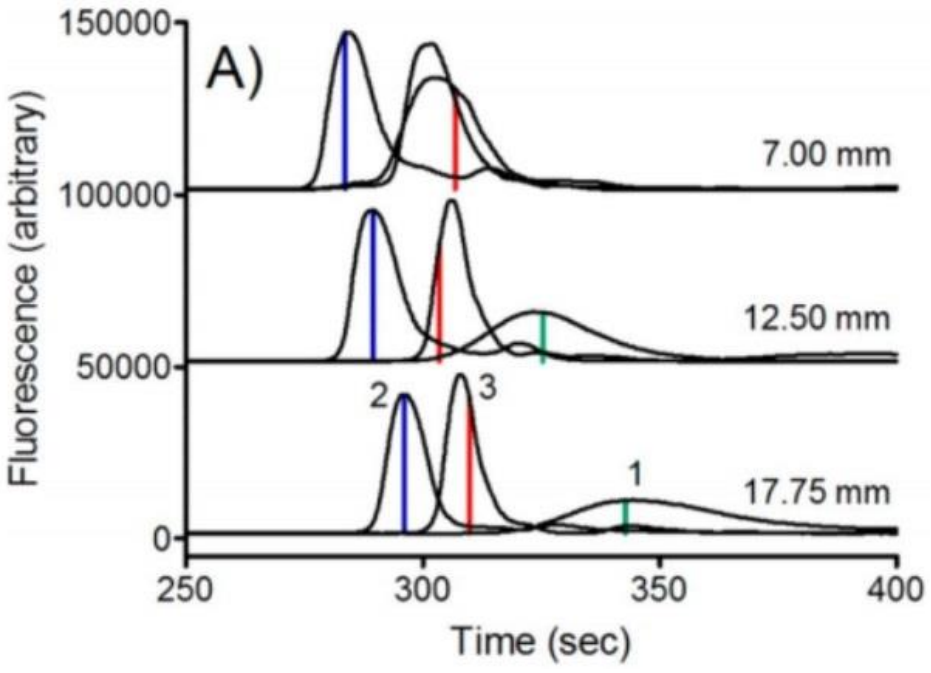

Fig. 1.21 – The figure shows the detection peaks as a function of time in case of dyes mixture separation: (1) Rhodamine 110, (2) Rhodamine 123, (3) Fluorescein. It is evident the time broadening due to surface adsorption. Indeed, the peaks width become larger over the time [40].

For example, the separation of a dye mixture composed by Rhodamine 123, Rhodamine 110 and Fluorescein performed by employing a glass μFFE chip with 25mM of HEPES (N-2-Hydroxyethylpiperazine-N'-2-Ethanesulfonic acid) buffer [40], it is clear that the width of the peaks increases with time.

The detection is performed for different distances along the separation chamber by employing a stereo microscope model Nikon AZ100. Moreover, the broadening effect behavior during the separation gives essential information about the interaction of the analytes with the substrate surface [40]. Summarizing, if free flow electrophoresis is performed in the microscale world, it is fundamental to choose the right material according to the nature of the analytes, which must be separated improving in such a way the separation performances by avoiding undesired effects. Considering the previous example, an excellent solution can be to substitute the borosilicate glass chip with one fabricated with ABS (Acrylonitrile Butadiene Styrene). Indeed, this material does not interact with rhodamine 123 and Fluorescein. On the contrary, Rhodamine 110 shows a little interaction with it. Thanks to such optimization, the time broadening is reduced in such kind of electrophoresis technique. Focusing on proteins separation process that involves p503 myoglobin and cytochrome c, the performances are degraded by the ABS and in this last case, it is better to employ a glass substrate.

1.7 Objectives statement

This work aims to propose a new μFFE device capable to isolate the exosomes biomarkers of the lung cancer useful to perform a liquid biopsy by exploiting a free flow electrophoresis process. The devices have been fabricated by using the 3D printing poly-jet technology. The main objective is to compare the printer performances in fabricating the μFFE chip in Glossy and Matte modes to determine if the first surface finished is better in term of printing accuracy and roughness with respect to the second one.

Another objective is to determine which are the best dimensions of the partitioning bars among different provided design solutions. The choice is made by analyzing the variation of the printing accuracy in case of the Glossy mode fabrication when the width of the bar is changed. The last objective is to determine which are the best separation parameters in terms of voltage, buffer

and sample flow rate to obtain the process confinement and the best separation in the case of the electrophoresis of a dye mixture composed by Bromophenol Blue and Xylene Cyanol FF performed by using one of the μFFE device.

2.

Materials and methods

2.1 The design

In this phase, the first objective is to focus the attention on the design and to describe in detail the chip. In particular the morphology of the μFFE device are analyzed (see Fig. 2.1).

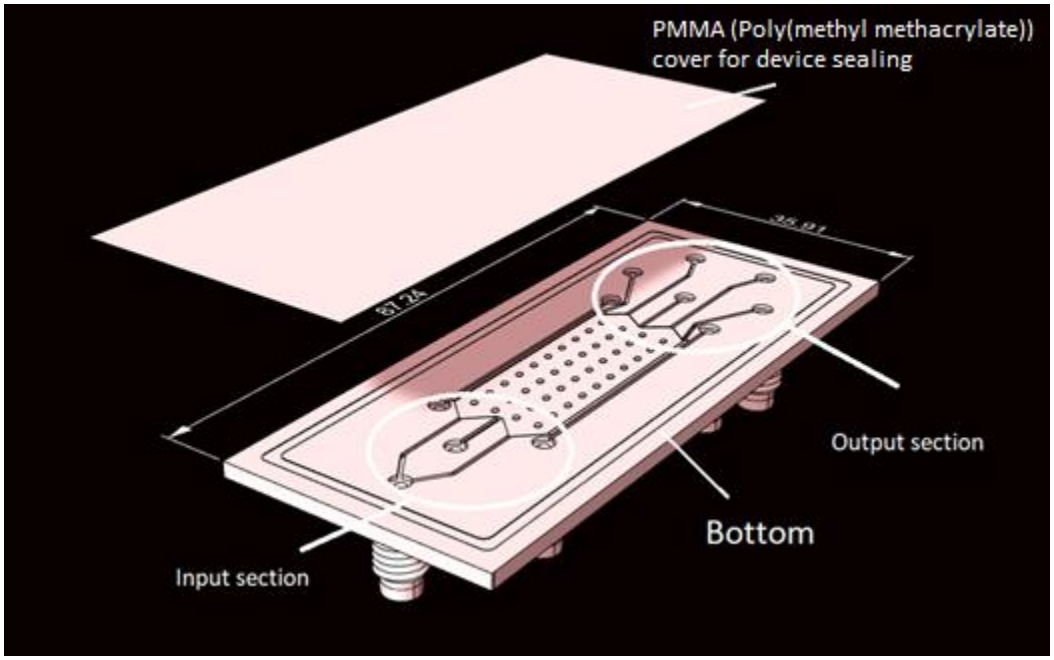

Fig. 2.1 – The picture shows the morphology of the μFFE device designed in Rhinoceros.

The second objective is to describe and analyze the fabrication process used to build the prototypes. The device proposed in this Master's thesis is a Lab-On-A-Chip (see Cap. 1) employed to perform the free flow electrophoresis at the microscale level simply and efficiently.
In such a device, the separation takes place in an accurately shaped microfluidic chamber (see Fig 2.2). This last one contains forty 100 μm high ellipsoidal pillars which have the role in preventing the cover from collapsing onto the chamber floor after the sealing of the device.

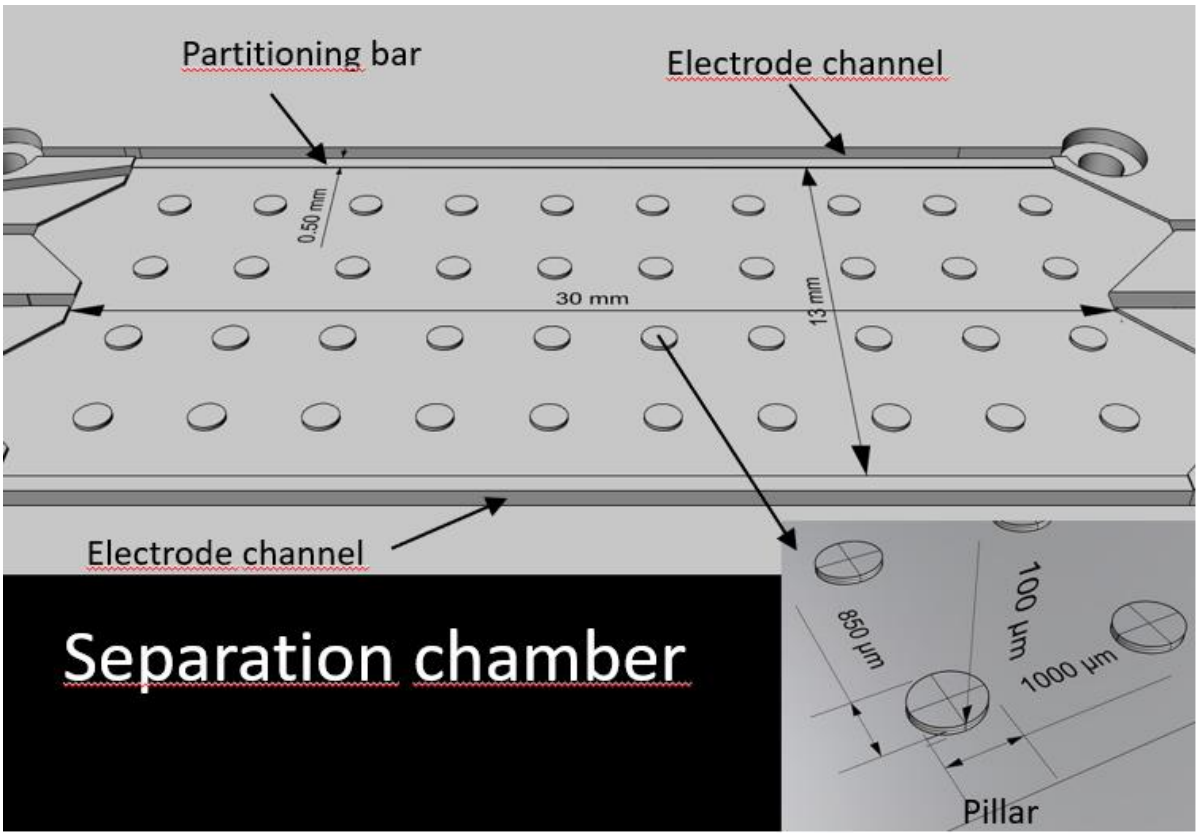

Fig. 2.2 – The picture shows a detailed view of the separation chamber.

The design of these particular features gives more stability to the whole chip. Moreover, the chamber is separated from the electrode channels by means of the use of two partitioning bars (see Cap. 2.1.3). As already cited, the μFFE technique consists of the application of an electric field directed perpendicularly with respect to the separation chamber. In particular, the electric field is generated and it is transferred to the chamber by using two stainless steel wires contained within two microchannels located on the chamber sides (see Fig. 2.2).
Analyzing more in detail, the device includes holes that serve to inject the fluid streams directly

inside the separation chamber. The chip is provided of four inlets: two are used to pump the sample solution and the buffer solution into the microfluidic chamber, the remaining two to pump the buffer solution into the electrode channels (see Fig. 2.3).

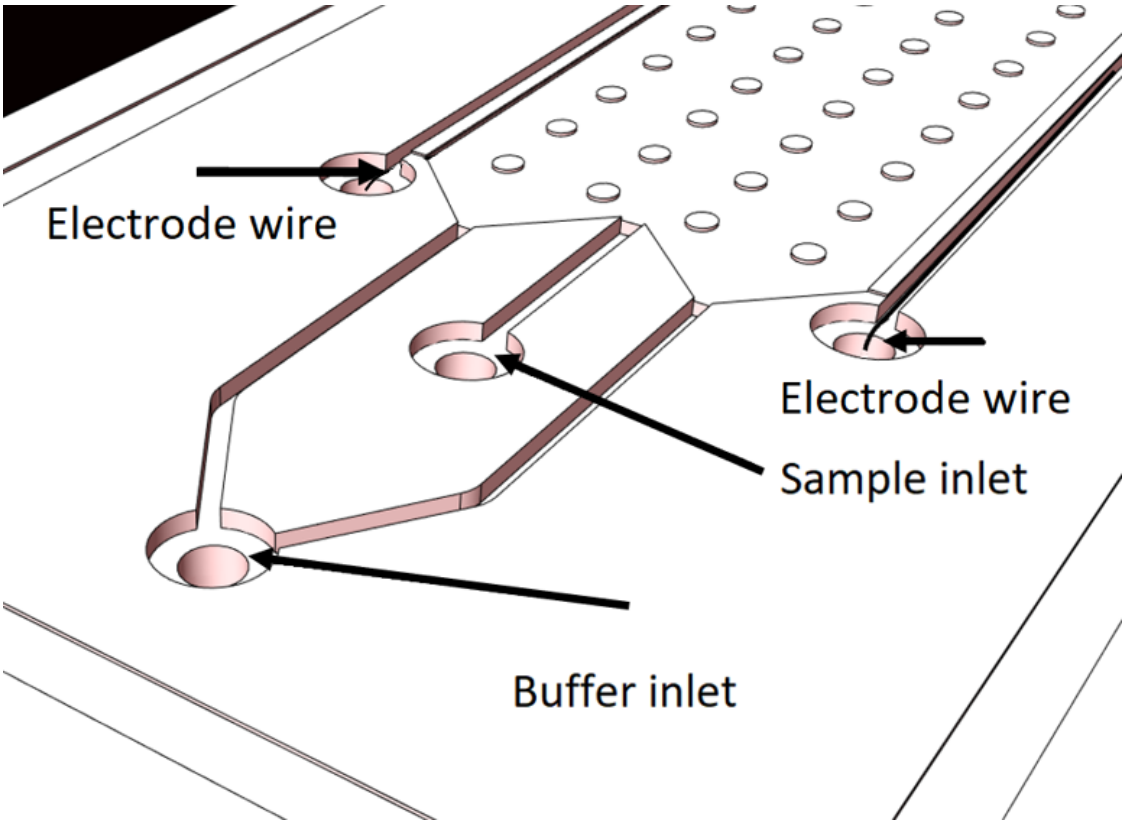

Fig. 2.3 – The picture shows a detailed view of the input section of the device.

On the other side of the chamber, an output section is used to collect the separation products obtained from the process (see Fig 2.1). In particular, the chip has seven outlets holes. Two are part of the electrode channels, while five serve to collect the results of the free-flow electrophoresis. The mechanical design of the μFFE chip is carried on using a commercial 3D computer graphic and CAD software called Rhinoceros. This software is based on the NURBS mathematical model, which offers a precise representation of curves, surfaces and solid onto a user-friendly design environment. In particular, this solution is preferred for its modularity and the possibility of managing the user interface in a versatile way, offering a 2D

and 3D efficient design solution in a unique environment.

Moreover, this software offers the possibility to create some design levels allowing the designer to carry on an efficient and well-organized mechanical design. In this work, the geometry of the chip is provided divided between a 2D and a 3D level.

In particular, by using Rhinoceros, only the bottom part of the entire Lab-On-A-Chip is designed (see Fig. 2.1).

Focusing on the design, the dimensions (see Tab. 2.1) are chosen as small as possible, allowing in this way to inherit all the advantages intrinsically present in the miniaturized microfluidic devices and to avoid the wasting of print materials employed during the fabrication process.

Feature	**Length CAD (mm)**	**Width CAD (mm)**	**Depth CAD (mm)**	**Diameter CAD (mm)**	**Volume CAD (μL)**
Chip	35.91	87.24	1.50	-	-
Separation chamber	30.00	13.00	0.10	-	39.54
Partitioning bar	13.00	0.50	0.05		
Pillar	1.00	0.85	0.10	-	-
Inlet/outlet channel	-	0.50	0.50	-	-
Inlet/outlet circle	-	-	-	2.69	-
Electrode channels	30.00	0.50	-	-	-

Tab. 2.1 – The dimensions of the μFFE device (see Fig 2.5).

The communication between the μFFE device and the macro scale world is obtained by implementing different standard fluidic connectors through which the sample and the buffer solutions are pumped into the separation chamber thanks to the use of a pumping system. In particular, the connectors are built on the back of the device (see Fig 2.4). In this way, the front of the chip where the separation chamber is located can be free from pipes and visible to the user.

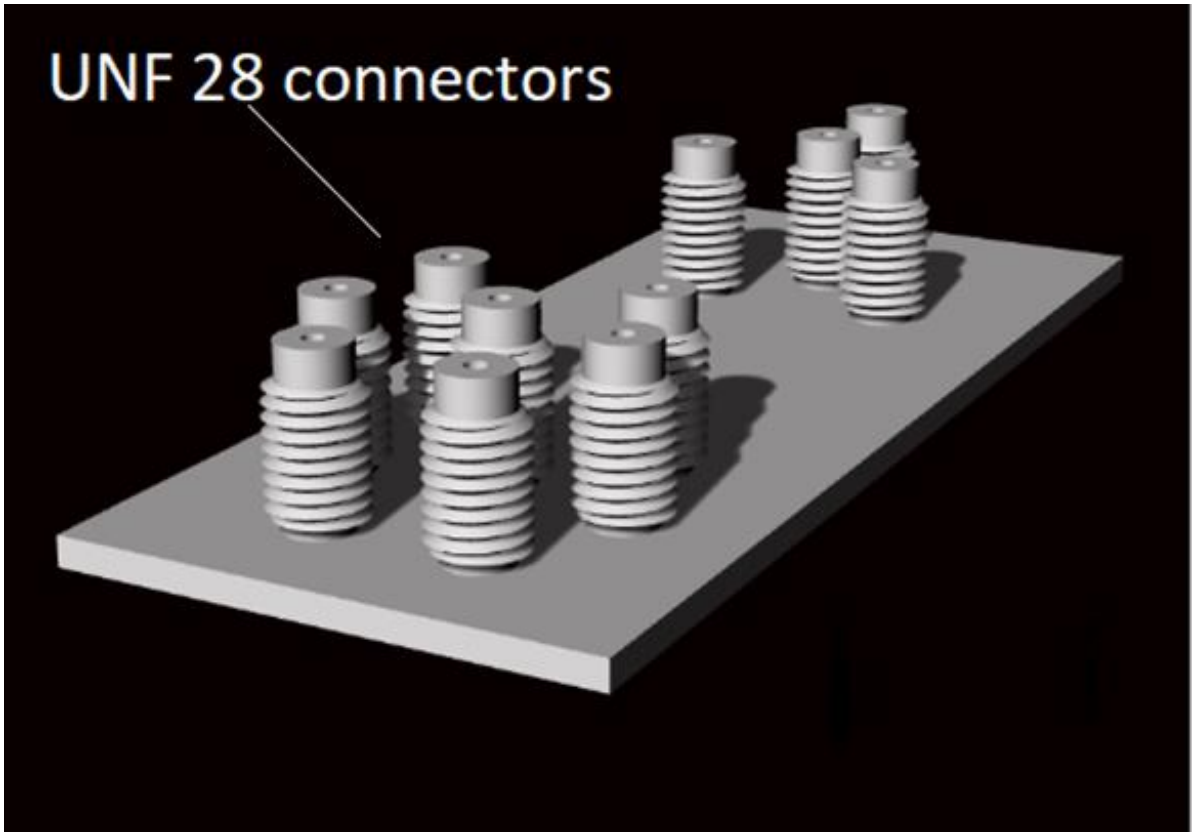

Fig. 2.4 – The picture shows a detail of the back of the μFFE device. In particular the standard UNF 28 threaded connectors.

The entire methodology starts with the creation of the 2D level. During the microfluidic design, several solutions to dispose of the inlet and outlet channels and holes must be tried to obtain an excellent aesthetic impact and waste the least area as possible. In particular, the inlet and outlet circles footprints are placed in positions (see Fig. 2.5) allowing in this way to connect easily the fluidic pipes to the inlet and outlet sections of the device: the required space to screw or fit them to the chip is assured by occupying as low space as possible.

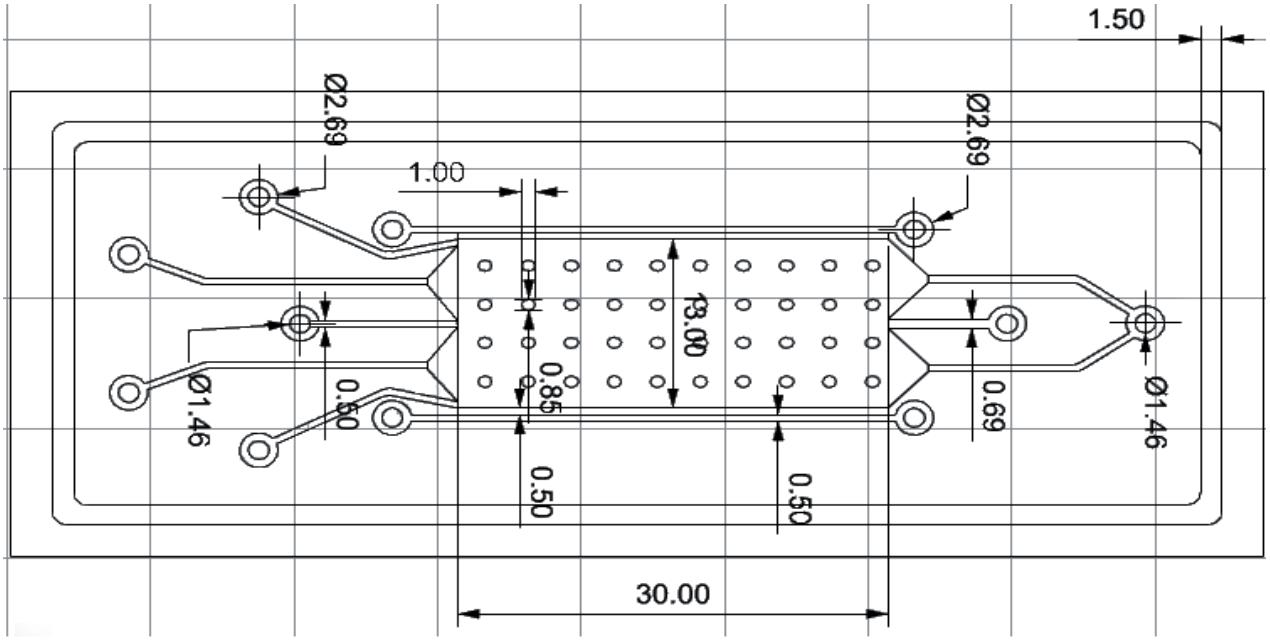

Fig. 2.5 – 2D mechanical draw of the μFFE. In particular, all the geometrical nominal CAD dimensions are represented by employing a mm scale (see Tab. 2.1).

Moreover, particular attention must be spent on positioning the channel curves. The angle of curvature must be chosen less than 45 degrees to avoid to have turbulent flows. This methodology guarantees the possibility to modify the entire chip dimensions by modifying the 2D model. Indeed, the chamber shape, the inlet-outlet hole diameters and the channel geometry can be changed to try new design solutions. The unit of measurement in the design plane of Rhinoceros is set to mm.

The 3D level of the μFFE device is built by starting from the 2D one. To carrying out the design, the single parts must be extruded singularly in the form of closed surfaces. Subsequently, the single features are merged to obtain the whole chip using the union, intersection and difference commands provided by Rhinoceros.

2.1.1 The partitioning bars design

As well known, one of the main problems of the μFFE devices stay in the generation of electrolysis bubbles [14]. In particular, they must be hindered to block them from entering inside the chamber and to avoid the perturbation of the separation process. There are different solutions to realize such kind of separation in a Lab-On-A-Chip. In the prototypes designed and fabricated during this master thesis, the integration of two partitioning bars has been preferred [19] with respect to mount a separation membrane. This choice's primary motivation lies in the more comfortable and faster manufacturing process, which allows to speed up the entire fabrication chain by avoiding to spent further time preparing and integrating a separation membrane. In the first designed prototypes, the nominal height of the bars has been fixed to 50 μm.

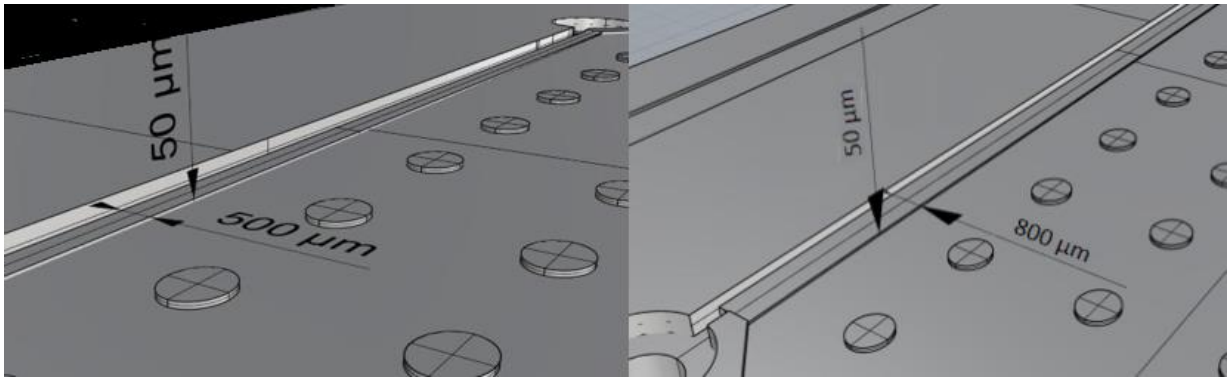

Fig. 2.6 – The picture shows two geometrical design solutions of the partitioning bars.

The fabrication results of the geometry provided by the 3D printer were accurate for the device printed in Glossy mode, but during the performance of separation tests, problems were encountered. In particular, the separation chamber has been invaded by the electrolysis bubbles demonstrating that the featured bars in this case were not enough to provide a stable separation. Therefore, other prototypes with wider or higher bars were designed to solve such problem. In particular, other alternatives solutions were designed. In the second one, 50 μm high and 800 μm wide bars were designed. Measurements were realized to analyze the variation of the accuracy of the 3D printer from passing from 500 μm to 800 μm bars. Since the results in terms of accuracy

were negative the width was fixed again to 500 μm. Therefore, to solve the bubbles invasion problem, further designs were realized by modifying the height from 50 μm to 70 μm but no analysis in such case was done due to force majeure (see Fig 2.6).

2.1.2 The device electrodes

The device is provided of two electrode channels which contain the wires necessary to apply the electric field. These are realized by using two stainless steel wires. This corrosion-resistant metal is chosen thanks to its quite low resistivity, which is $\varrho = 0.69\ \mu\Omega/m$ at room temperature. However, the two electrodes and the cables which are employed to connect the device to the power supply, contribute to degrade the applied voltage by introducing a parasitic resistance. The electrical resistance introduced by the electrodes can be estimated. Knowing that the average length of the wires is around 25 cm and knowing the section which is equal 150 μm the electrical resistance is computed as:

$$R = \rho \frac{L}{S} \tag{1.13}$$

Therefore, substituting these values, the obtained resistance is $R = 1.15\ m\Omega$.

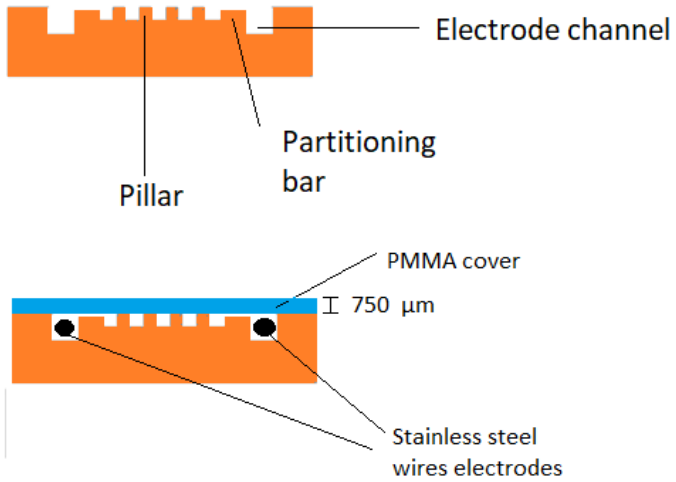

Fig. 2.7 – This picture shows a representation of the device section of the open and the sealed device.

2.1.3 The connectors

The first designed prototypes mount on board 18.70 mm long Luer slip connectors (see Fig. 2.8) which were designed directly in an appropriate level of the Rhinoceros project. The Luer slip is a standard connection widely employed by many companies and laboratories to realize a leak-free small-scale fluidic fitting.

Fig. 2.8 – The picture shows the 18.70 mm Luer slip connector.

In particular, it is employed as a standard connector in syringes. This standard-fitting is realized in plastic or metal according to the needs. The features are contained in the standard ISO 594, DIN 1707:1996 and EN205941:1993.

This connector has a tapered shape, the opening angle from the mid axis of the cone is equal to 1.72 ° while the slope is equal to 0.03 mm/mm. The fluidic fitting is guaranteed by the friction force generated among the male and female parts. In a second designed μFFE prototype, the heights of the Luer slip connectors are reduced to 2.9 mm (see Fig. 2.9), allowing to save in such way dead volume passing from 31.307 μL to 4.855 μL. The employment of shorter connectors allows to save 84.5% of dead volume. However, in this case, the connections do not seal enough, introducing pressure variations and leaks in the device, therefore this solution was discarded.

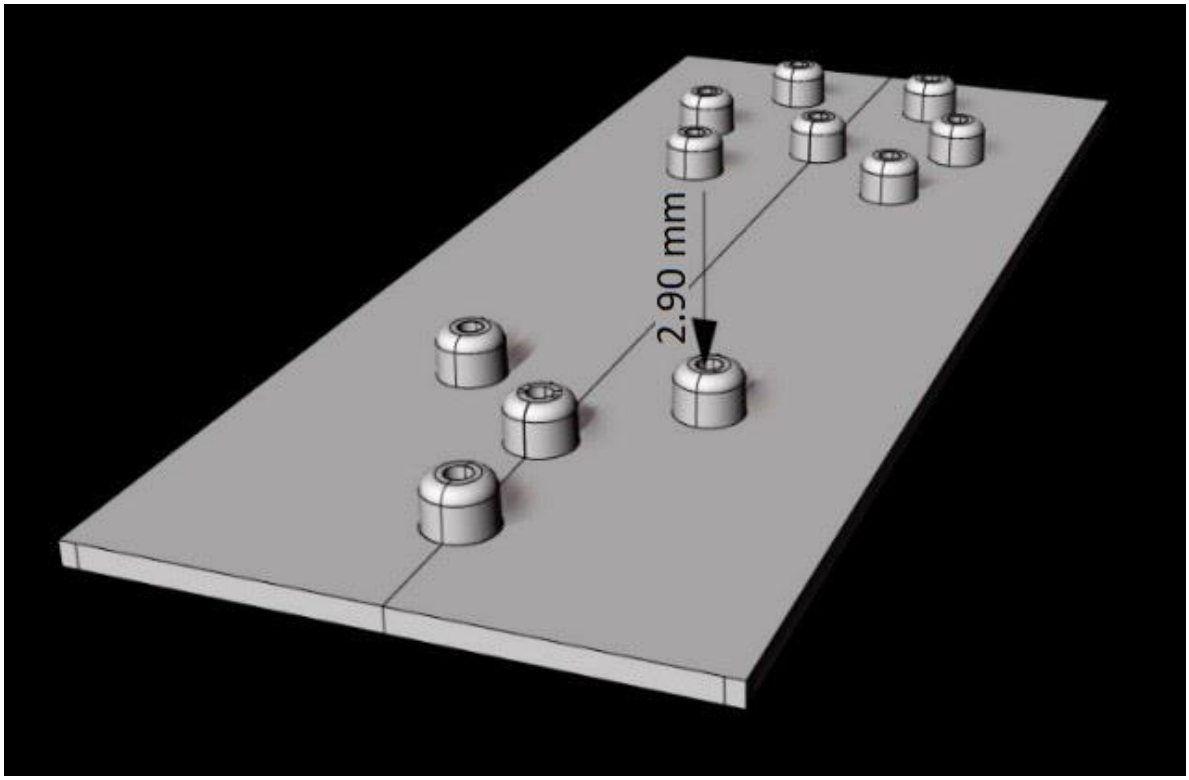

Fig. 2.9 – Back of the device: 2.9 mm Luer slip connectors.

Another advantage of reducing the dead volume is correlated with time. Indeed, for example, if the sample flow rate is equal to 2 μL/min, the time to fill the entire volume of the connector 18.70 mm long is equal around 16 minutes. On the contrary, only 3 minutes is enough to fill the 2.90 mm long connectors.

In a third design, the device was modified. In particular, it was maintained equal to the previous one concerning the chamber, the electrodes and the partitioning bars dimensions, but the Luer slip connectors were replaced with 11.50 mm long standard UNF 28 ¼" male threaded connectors (see Fig. 2.10). The UNF is an acronym that stands for unified national fine thread. The number 28 indicates the screw threads per inch. The design was realized directly in 3D as a singular part, the integration with the device was performed in a subsequent phase.

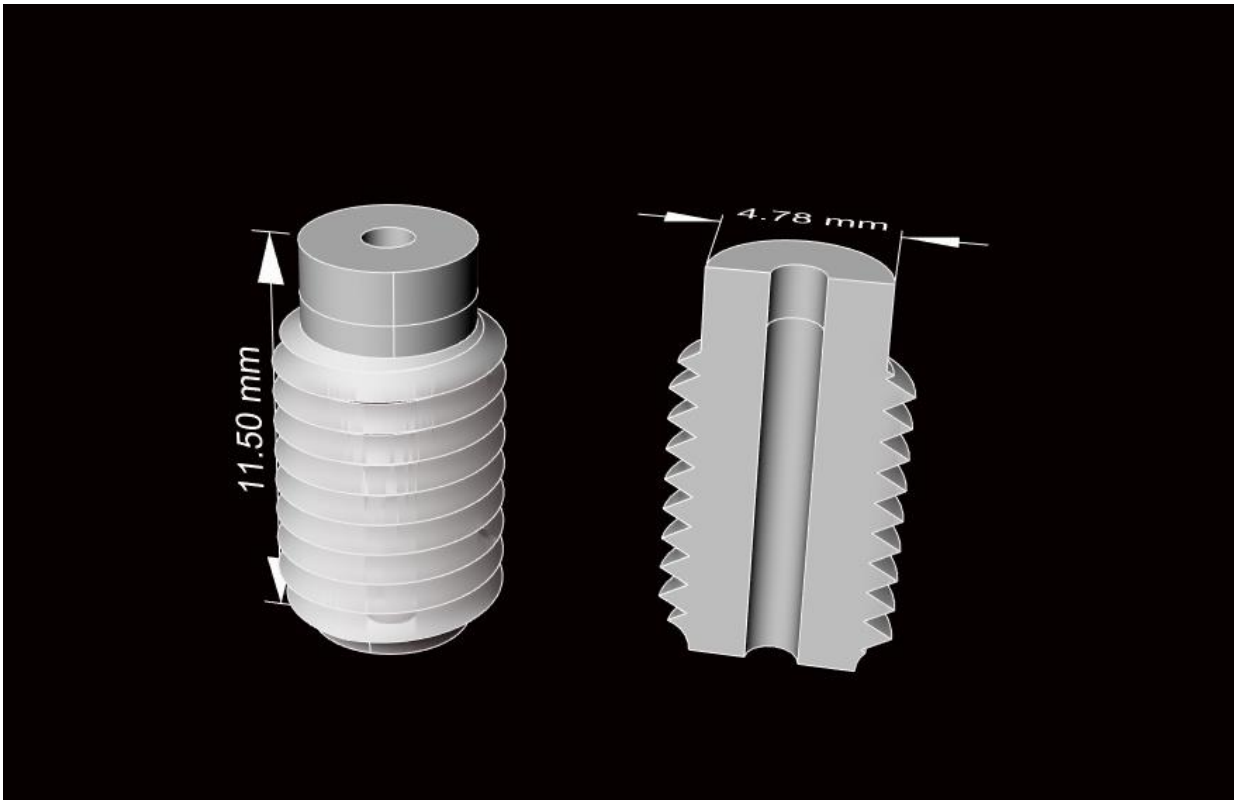

Fig. 2.10 – The picture shows a 11.50 mm long UNF 28 connector.

These connectors, thanks to the threaded screw, guarantee a robust fitting of the tubes to the inlets and outlets of the device by avoiding load losses and pressure variations.

2.2 Device fabrication

The final goal of this section is to describe the fabrication method of the μFFE Lab-On-A-Chip of this master thesis. The fabrication process is very simple and can be performed faster with respect to the conventional micromachining techniques, which require expensive processes and special equipment. The whole building recipe can be summarized in four steps: 3D printing, cleaning procedure, electrodes insertion, device sealing.

2.2.1 3D printing of the μFFE

The μFFE chip has been fabricated by employing the 3D printing technique. In such case, it is possible to manufacturing a microfluidic chip without implementing slow and high-cost processes or master fabrication [21] [23]. The final file obtained in the CAD is in the .STL (stereolithographic) format. It is converted by the 3D printer into a low-level language interpretable from the machine. The original 3D geometry is divided by the 3D printer into 2D layers, by using optimized slicing algorithms. Different 3D printing techniques can be employed, such as stereolithography (SLA) inkjet, fused deposition modeling (FDM) and laminate object [43]. In this work, the bottom of the device (see Fig. 2.1) was built by employing a 3D printer model OBJET 30 provided by Stratasys (see Fig. 2.11).

Fig. 2.11 – The Chilab's OBJET 30 3D printer.

In particular, it is a high performances machine based on the poly-jet technology. In this technique, the prototype is built by extruding layer by layer and by curing the build under the exposition of an UV lamp. This technique is very precise and a good variety of materials are available [44].

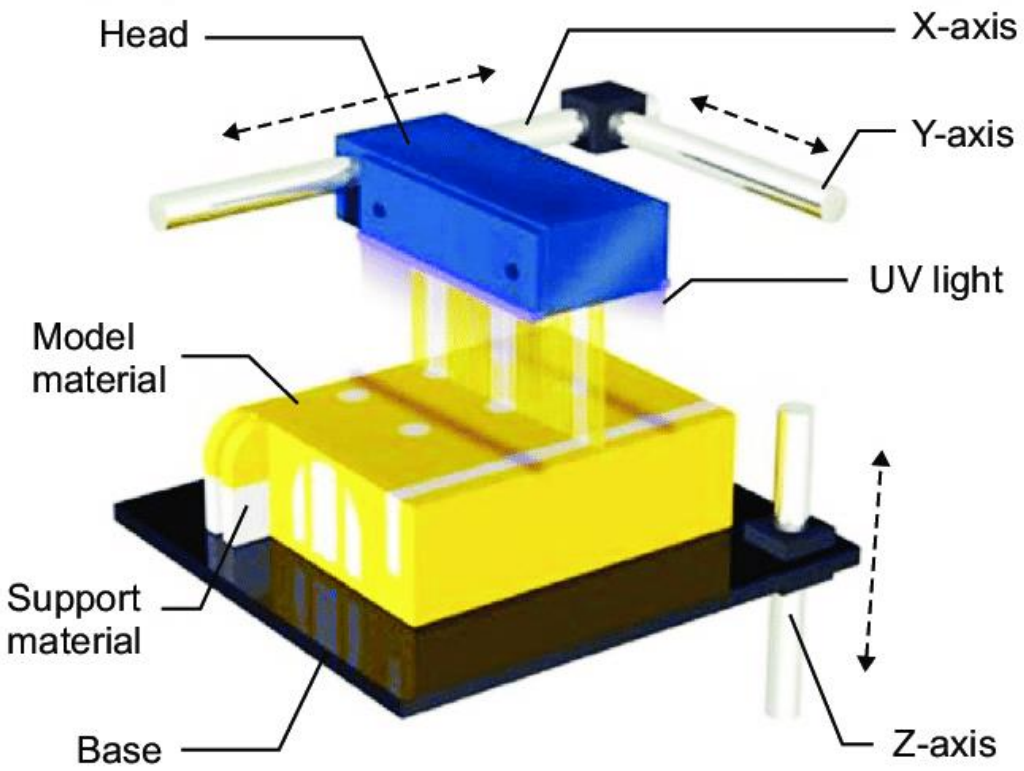

Fig. 2.12 - PolyJet 3D printing technique [44].

In such a technique, a liquid photopolymer is distributed through a printing head in the XY plane and solidify under the illumination of a UV lamp. In such a way, very thin fabrication layers are created on the Z-axis direction. In particular, during the printing process, the build tray moves down after the deposition of one layer. Thanks to such technique, the object is built adding layer by layer along the z axis until the end of the entire printing process. A considerable quantity of materials with different properties is available to be employed for the OBJET 30. In particular, different kinds of photopolymers can simulate the characteristics of some material. The μFFE device of this master thesis was built by using two polymers. The first one is a structural resin

provided by Stratasys (VeroWhitePlus RGD835) [45], while the second one serves as sacrificial material (SUP705) [45] to support the structure during the device fabrication. Focusing on the OBJET 30, it offers the user two available printing modes which provide a different surface finished.

- **Glossy**

  The prototype is built by employing the resin VeroWhitePlus RGD835 as structural material and the SUP705 as support material where is needed to sustain the building. In this mode, the surface finished is reflective and smooth to the touch.

- **Matte**

  In this mode, the object is fabricated by employing the support material. In this case, the surface finished is non-reflective and rough to the touch.

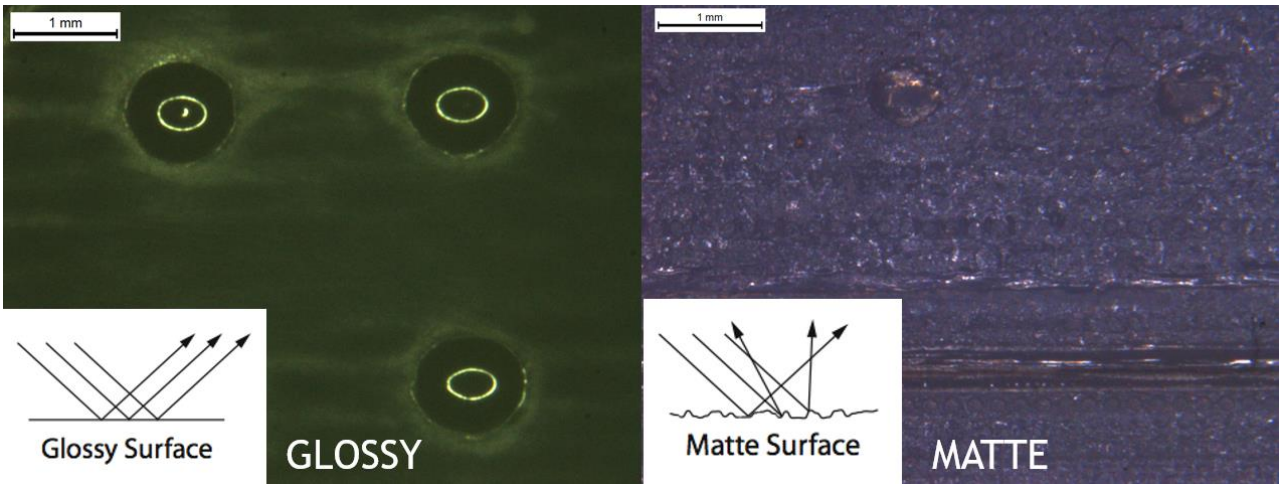

Fig. 2.13 – The picture shows the internal part of the separation chamber for one Matte and Glossy surface finished prototypes. The Matte surface finished is full of microdefects.

The characteristics of the 3D printer are stated in the table:

OBJET 30	Value
Build resolution X x Y x Z (dpi)	600 x 600 x 1600
Maximum build size (mm)	294 x 192 x 148.6
Layer thickness along z axis	28 μm by using the Verowhiteplus RGD835 resin
Lateral resolution	42 μm

Tab. 2.2 – OBJET 30 characteristics [46].

Before to start the printing of the prototype, a boot routine must be performed to ensure the correct initialization of the printer and to avoid poor print quality.

1. The first step consists of the verification of the printing heads cleaning. For this purpose, a pattern test must be performed in order to extrude some material onto a paper sheet to assure that the nozzles work in the right way.
2. If the pattern test failed, the printing head and roller must be cleaned using the 2-isopropanol purchased by Sigma Aldrich and a special cloth.
3. After the verification of the printing heads cleaning state, a purge sequence must be performed in order to clean the nozzles and remove residues released from the previous prints.
4. After the purge sequence execution, another pattern test must be performed again to verify the heads cleaning. If the test is positive, the printer is ready.

2.2.2 Prototype cleaning

After the end of the printing process, the fabricated device is collected from the OBJET tray. In this phase, the device is surrounded by the support polymer (SUP705), which has been employed by the 3D printer to build correctly the structure. Therefore, the first step of the cleaning procedure consists in the removal of the support material by using a water-jet station (see Fig. 2.14).

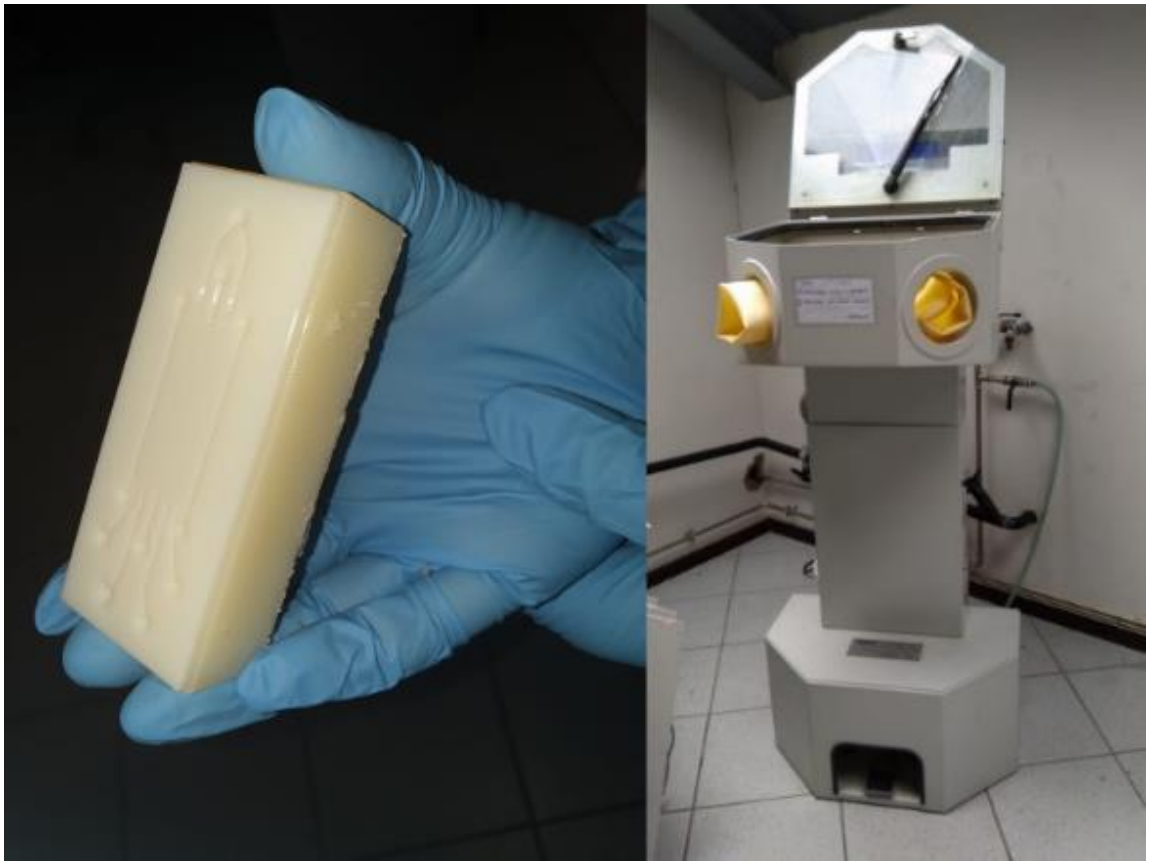

Fig. 2.14 - Device cleaning by using a waterjet station.

The pressure of the jet inside the chamber must be finely tuned, especially in the case of connectors cleaning to avoid damaging the prototype. After removing the support material, the device is intensively cleaned by using water and 2-propanol (isopropyl alcohol) purchased by Sigma-Aldrich and dried using compressed air. Particular attention must be spent to clean the microfluidic chamber obtaining a perfect cleaned chip (see Fig. 2.15).

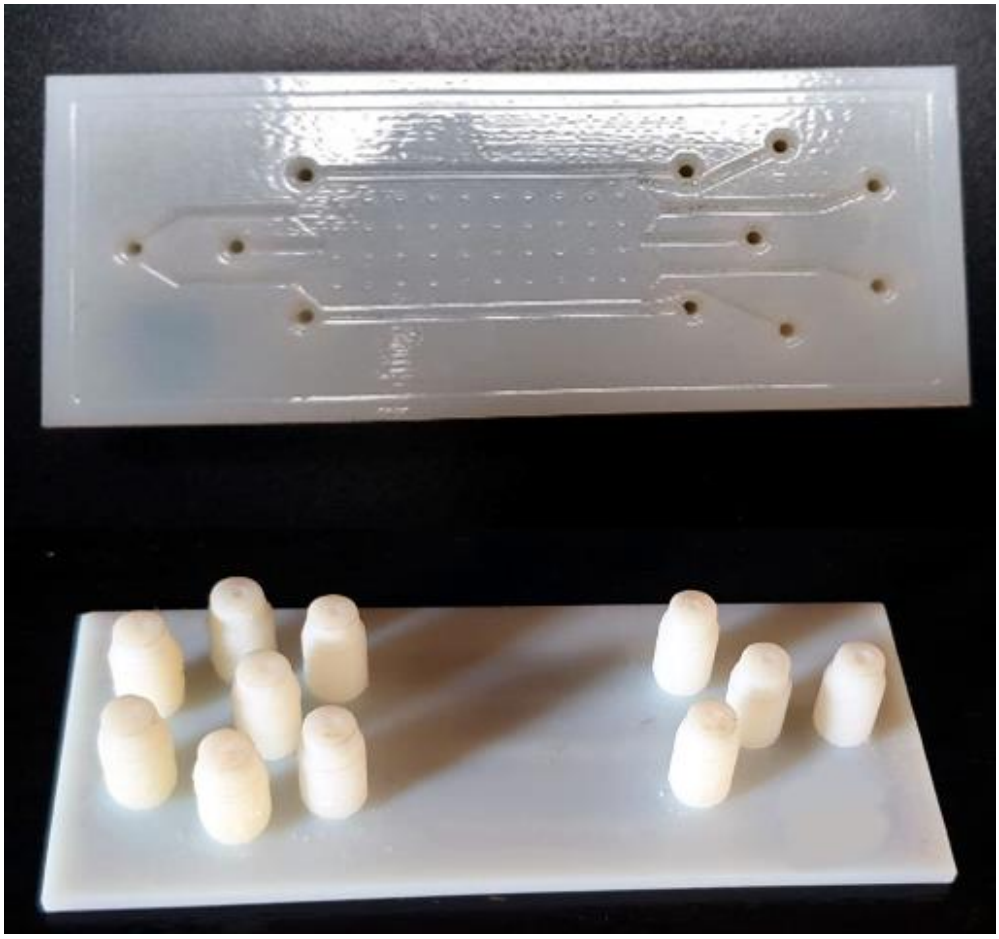

Fig. 2.15 - The 3D printed bottom part of the μFFE device after the cleaning procedure.

Moreover, in the case of a prototype which mounts onboard threaded connectors, a particular delicacy must be used to clean them with a toothbrush being careful not to strain them since they are the most fragile parts of the device.

2.2.3 Device sealing procedure

The sealing is one of the most crucial steps of the entire fabrication process. Indeed, the fabricated μFFE chips must be sealed in order to have a precise closed volume capable to confine sample and buffer and prevent contaminations.

The material selected for realize the cover of the printed prototypes was 750 μm thick PMMA (Poly(methyl methacrylate)). It is chosen in substitution to other transparent materials like the

glass thanks to its great features such as compatibility with electrophoresis, optical transparency, shatter resistance, lightweight, scratch resistance. Moreover, it exhibits favorable patterning process. Indeed, it can be manufactures in a simply way by cutting manually the desired piece by using a common cutter. Different bonding techniques can be implemented according to the literature to seal a microfluidic device. In this work the μFFE chip is sealed by exploiting a thermal assisted adhesive bonding technique realized by using the resin PEGDA 575 with 1% IRGA CURE 819 to attach the PMMA slice to the device substrate (fabricated with VeroWhitePlus RGD835) (see Fig. 2.16).

Fig. 2.16 - The picture shows the device parts on the left and the sealed device on the right.

This bonding procedure offers some advantages with respect to exploit other techniques such as purely thermal or laser assisted bonding which need higher temperature or expensive equipment to be realized [47]. This technique can be exploited in a simply way by using a common laboratory hot plate maintaining a low process temperature. Moreover, it is fundamental to set properly the temperature in order to have a good bonding without to damage the geometry and

melt the device. The drawback in employing this sealing technique is that the thickness of the adhesive layer is not well controlled and could leads to voids in the final result if particular attention is not spent. In particular, the mixture must be spread around the microfluidic channels by taking care to not drip resin into the chamber. Moreover, this step must be performed under the illumination of a yellow light to avoid a premature polymerization of the resin due to the exposition to the light. The two stainless steel wires are inserted manually inside the two electrode channels. Subsequent the adhesive layer is sprayed on the substrate and the cover is manually placed over the chamber. The PMMA sheet is gripped to the device by using a series of clips. Two combinations of time and temperature are tried. The first bonding recipe is performed at low temperature T = 60° C for 1 hour. The obtained result is good but too much time is employed slowing down the manufacturing process. For this reason, a second bonding recipe better tuned was performed by allowing in such a way to save time. In this new one the temperature was increased to T = 120 °C and the time employed was reduced to 20 minutes.

3.

Fabrication process results analysis

In this section, efforts are dedicated to conduct a deep analysis of the fabricated μFFE devices. Prototypes of the microfluidic chip were printed by employing the two fabrication modes of the OBJET 30 (the Glossy and the Matte one) (see Cap. 2.2.1). In particular, several measurements were realized for each feature dimension of the prototype and a statistical analysis was performed to analyze the 3D printer accuracy in both cases. The N measurements were employed to computer an average value and its error. This last was obtained by computing the standard deviation.

$$\bar{x} = \sum_{i=1}^{N} \frac{x_i}{N} \tag{3.1}$$

$$\sigma = \frac{\sum_{i=1}^{N}(x_i - \bar{x})}{N} \tag{3.2}$$

Then analysis was realized by comparing, for each features dimension of the chip, the average value with the nominal value which has been set on the CAD to determine which surface finished mode was more accurate during the fabrication and respected better the reference value. Moreover, accuracy analysis of the 3D printer performances in fabricating 500 μm and 800 μm wide

bars in the case of the Glossy mode were realized. All the measurements and the pictures concerning the device features in the 2D plane were realized by employing an optical microscope (Leica VZ80C) (see Fig. 3.1) driven by its software.

Fig. 3.1 - Tencor P10 surface profiler and Leica VZ80C optical microscope.

The pillars and the partitioning bars height measurements were realized in a cleanroom by employing a surface profiler (Tencor P-10 Surface Profiler) (see Fig. 3.1).

3.1 Partitioning bars results

First of all, measurements were realized for the partitioning bars height of the Glossy and Matte devices by sampling in different points of the partitioning bar through the surface profiler. (see Tab. 3.1)

Partitioning bar	Glossy mode P10 height (μm)	Matte mode P10 height (μm)
Sample		
1)	54.79	58.74
2)	55.36	46.55
3)	50.6	41.03
4)	55.36	72.91
5)	59.86	71.92
6)	54.85	52.37
7)	45.35	39.37
8)	57.31	64.1
9)	48.08	39.5
10)	49.22	50.61

Tab. 3.1 – Partitioning bar height measurement samples for Matte and Glossy surface finished.

The average value and the standard deviation (uncertainty) for the height were computed. Ten samples have been taken on two glossy and on two matte surface finished devices. The profiles of the bar provided by the P10 in the two modes were acquired (see Fig. 3.2 and 3.3).

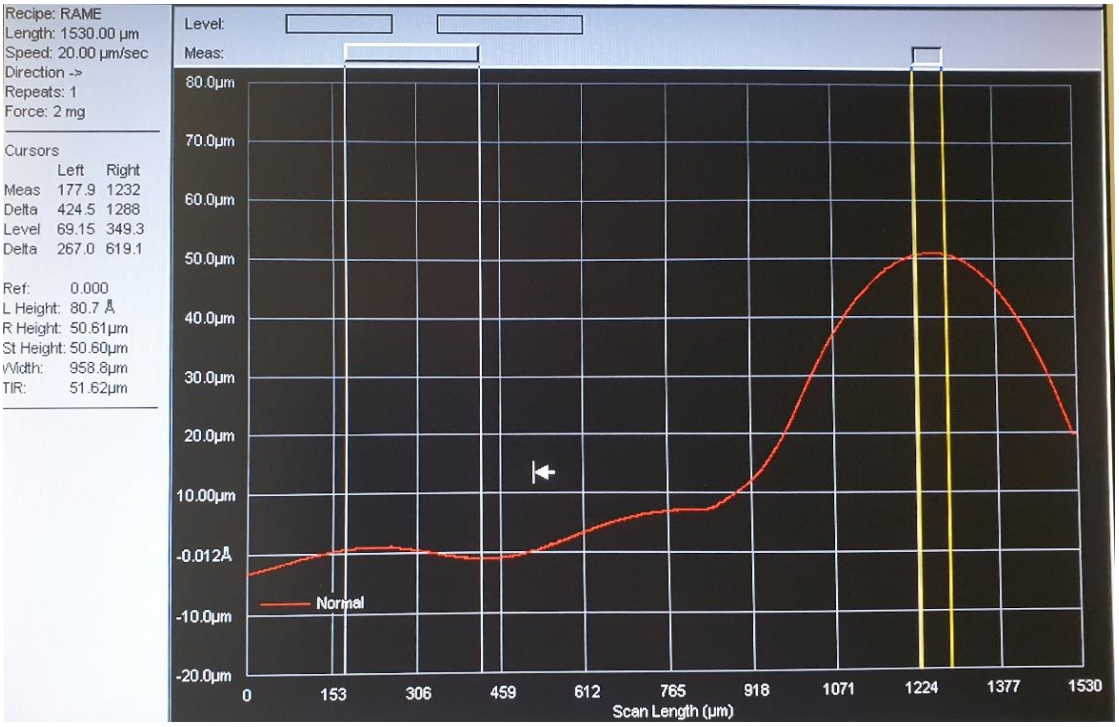

Fig. 3.2 – The photo shows the height measurement for the sample number 3 for the partitioning bar of a Glossy fabricated device at the surface profilometer.

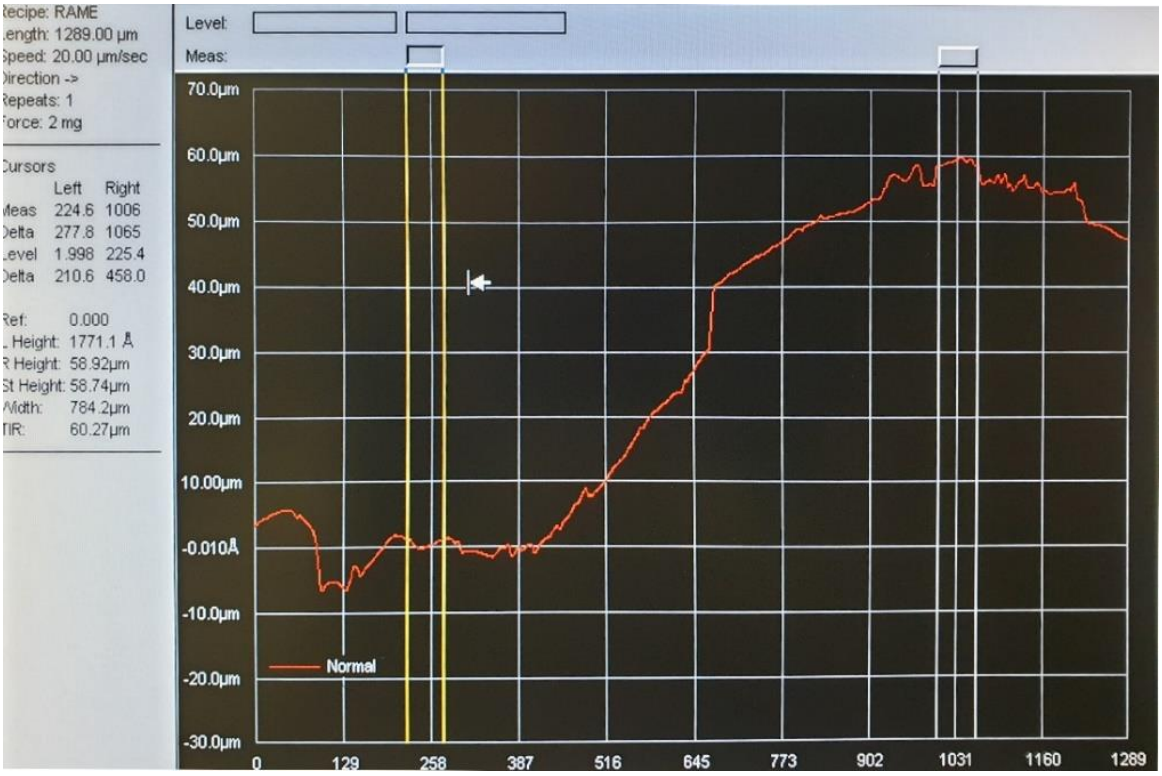

Fig. 3.3 – The picture shows the height measurement for the sample number 1 for the partitioning bar of a Matte fabricated device at the surface profilometer.

Subsequently width measurements on the partitioning bars were performed. They were realized in different points distributed along the length of the bar by taking twenty samples for four Glossy finish devices and ten sample for one Matte finish device (see Fig. 3.4 and 3.5).

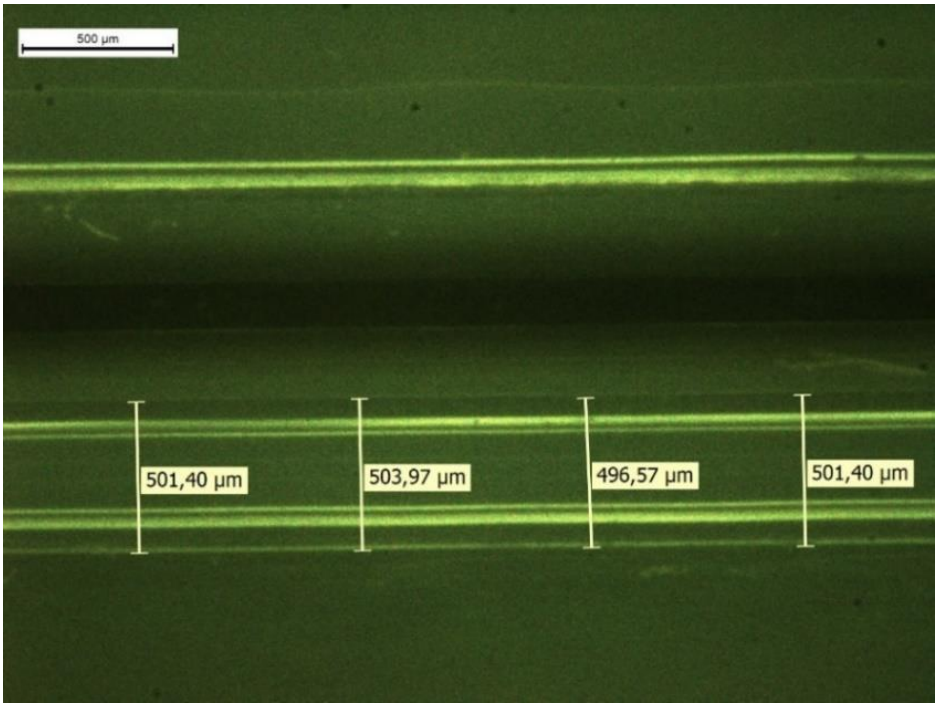

Fig. 3.4 – The figure shows measurement realized at optical microscope along the length of the 500 µm wide partitioning bar of a Glossy device.

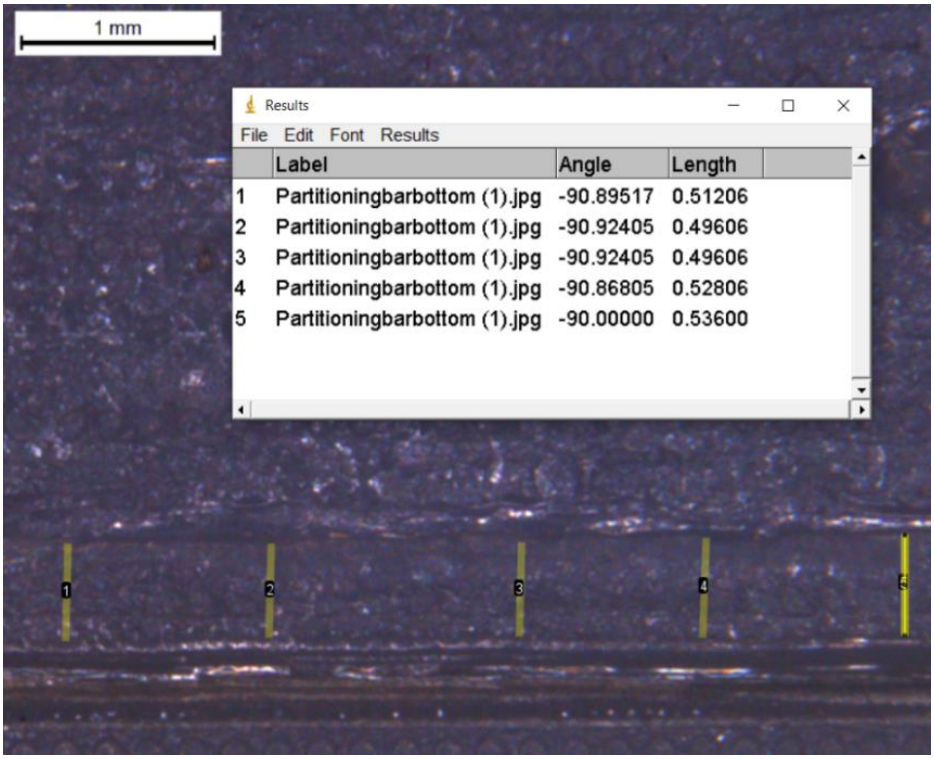

Fig. 3.5 – The figure shows measurement realized at optical microscope along the length of the 500 µm wide partitioning bar of a Matte device.

The average value and standard deviation for the height and width measurements are resumed in the Tab. 3.2.

Features	Dimension	CAD width (μm)	Glossy actual (μm)	Matte actual (μm)
Partitioning bar	Width	500	497 ± 4	522 ± 18
Partitioning bar	Height	50	53 ± 5	57 ± 11

Tab. 3.2 – Partitioning bar width and height average values and uncertainty (standard deviation) for Matte and Glossy surface finished.

Focusing on the partitioning bar height, in the Glossy surface finished case, the average value is 53 μm and it is closer to the nominal CAD value (50 μm) with respect to the Matte mode in which the average value is equal to 57 μm (see Tab. 3.2). Therefore, the accuracy in the first case is equal to 6% while in the second case to 14%. Moreover, concerning the Matte mode, the average mean error (standard deviation) is higher, this is due to the higher surface roughness of this surface finished. The fabrication results for the width are again better for the glossy mode since the average value (497 μm) is closer to the nominal CAD value (500 μm) with respect to the Matte case (522 μm). The accuracies are 0.6% and 4.4% respectively. The fabrication in this last mode shows a greater average mean error that is due to the over-extrusion of the 3D printer. Summarizing, the Glossy mode is the best one for fabricate the partitioning bars since the obtained results are more accurate both for width and height. Subsequently, a different analysis was performed. Measurements of width were realized only for Glossy devices which have 500 μm and 800 μm wide partitioning bars to analyze the 3D printer performance in the case of such width modification. The measurements were realized as in the previous case by taking the measurements in different points along the bar's length and computing the average and the standard deviation for two Glossy prototypes which have 800 μm wide bars and for four Glossy prototypes which have 500 μm wide bars by acquiring ten sample for each device (see Tab. 3.3).

Features	Dimension	CAD width (μm)	Glossy actual (μm)
Partitioning bar	Width	500	517 ± 3
Partitioning bar	Width	800	878 ± 8

Tab. 3.3 – Partitioning bar width average values and uncertainty for 500 μm and 800 μm reference values.

There is an evident decrease in printing accuracy for the 800 μm width case (accuracy of 9.75 %) since the difference between the average value and the reference one is higher with respect to 500 μm case (3.4 % accuracy). Moreover, the standard deviation is higher in the 800 μm case. Summarizing, it is better to maintain 500 μm width for the partitioning bar fabrication to avoid losses of 3D printer accuracy during the printing.

3.2 Pillars results

In order to prevent the cover from collapsing on the microfluidic chamber, some pillars are fabricated to improve the structural stability. (see Fig. 2.4) Therefore, it is interesting to observe how the OBJET 30 behaves during the manufacturing of such features. Measurements of the pillars in different points of the chamber were realized. (see Tab. 3.4) Furthermore, measurements of the same pillar were taken several times before to accept the value in order to be sure that the tip of the profilometer was located exactly in the center of the pillar to measure in such a way the maximum height. (see Fig 3.6 and 3.7). The profile of the pillar fabricated in Glossy has a better shape with respect to the Matte one that presents defects in the geometry (see Fig. 3.9).

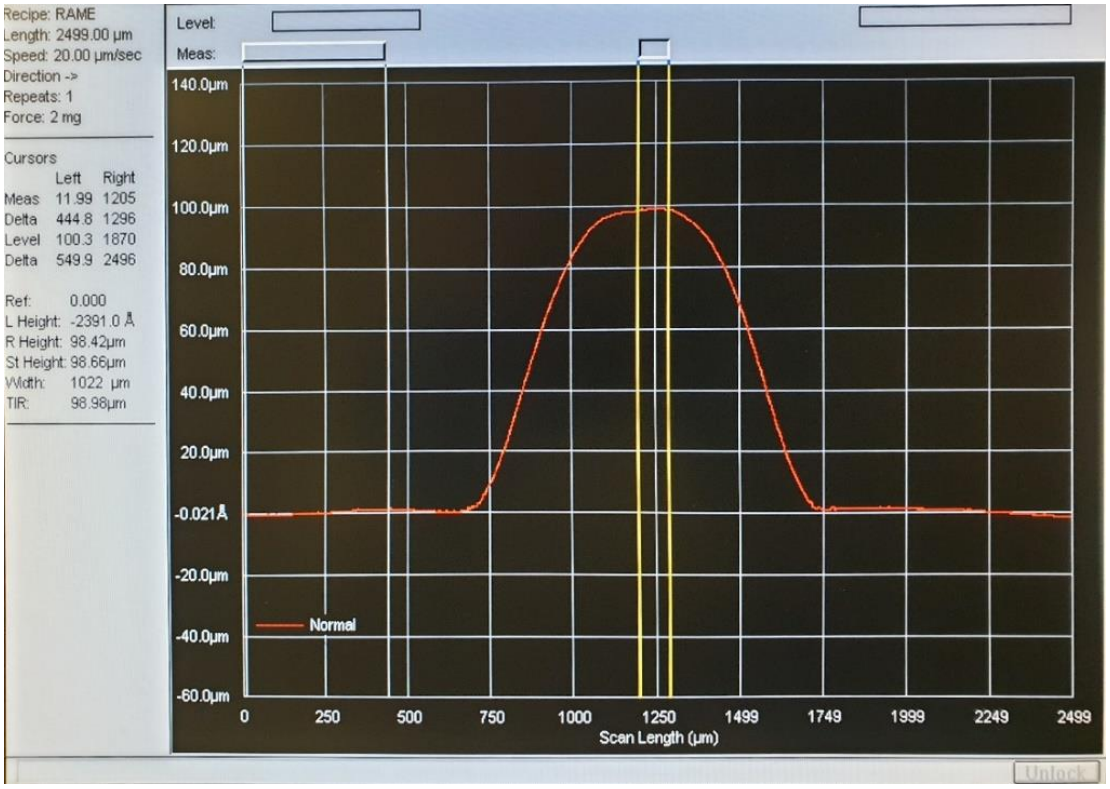

Fig. 3.6 – The figure shows the pillar profile for a Glossy fabricated device.

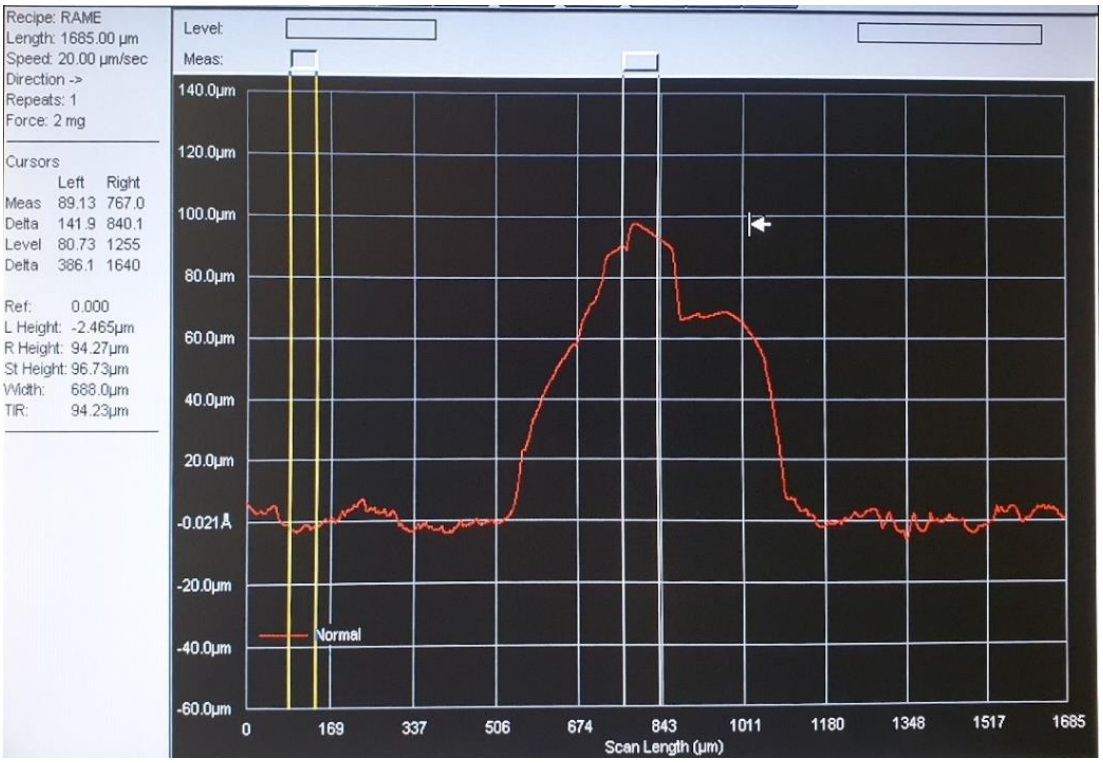

Fig. 3.7 – The figure shows the pillar profile for a Matte fabricated device.

The pillar's height of the devices fabricated with both modes were analyzed such as done in the partitioning bars case, to compare the 3D printer performances and determine which surface finished was more accurate for fabricate these features. The averages values with corresponding errors (standard deviations) for the height measurements are resumed in Tab 3.4. Ten samples were acquired for a Glossy and ten sample for a Matte device. The height of such features is more accurate in the Glossy mode since the average value (100.397 μm) is practically equal to nominal value (100 μm). The accuracy is equal to 0.4%. Moreover, the dispersion is very small. On the contrary, the average value for the Matte mode is quite far from the CAD one (accuracy of 18 %). Subsequently, other measurements were performed by taking ten width and length samples for one single Glossy device and five width and length samples for one single Matte device (see Fig. 3.8 and 3.9). The fabrication performances of the Matte mode concerning the pillar length and width were not satisfactory since the average values are quite far from the nominal one provided by CAD (1000 μm for the length and 850 μm for the width). In particular the accuracy of the pillar length of the Matte device was around 20% with respect to 1.5 % of the Glossy finish. The accuracy of the printer in respect pillar width for the Matte mode is around 15% compared with the only 0.7% of the Glossy finish.
Summarizing, the μFFE device print in Glossy surface finished shown better performances concerning the pillars manufacturing with respect to the Matte surface finished.

Features	**Dimension**	**CAD (μm)**	**Glossy actual (μm)**	**Matte actual (μm)**
Pillar	Height	100	100 ± 2	82± 6
Pillar	Length	1000	985 ± 18	801 ± 46
Pillar	Width	850	856 ± 10	725 ± 46

Tab. 3.4 – Pillar results for Glossy and Matte devices (average and standard deviation values).

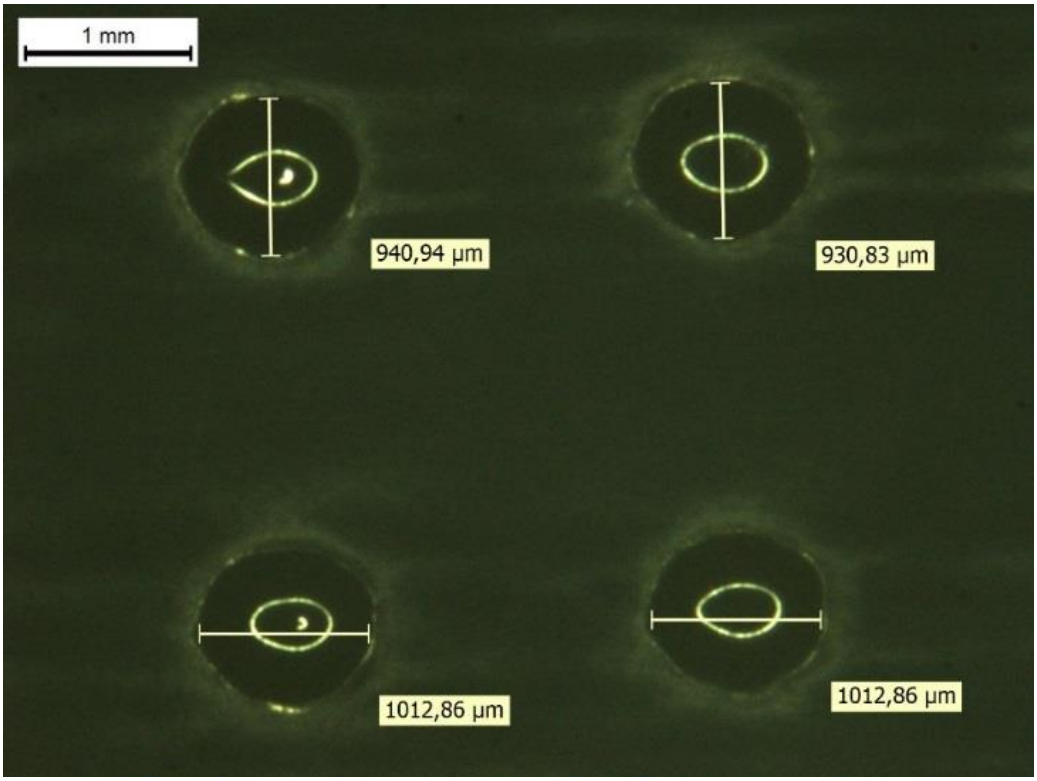

Fig. 3.8 – Samples of Pillar length and width for a Glossy device acquired at the optical microscope.

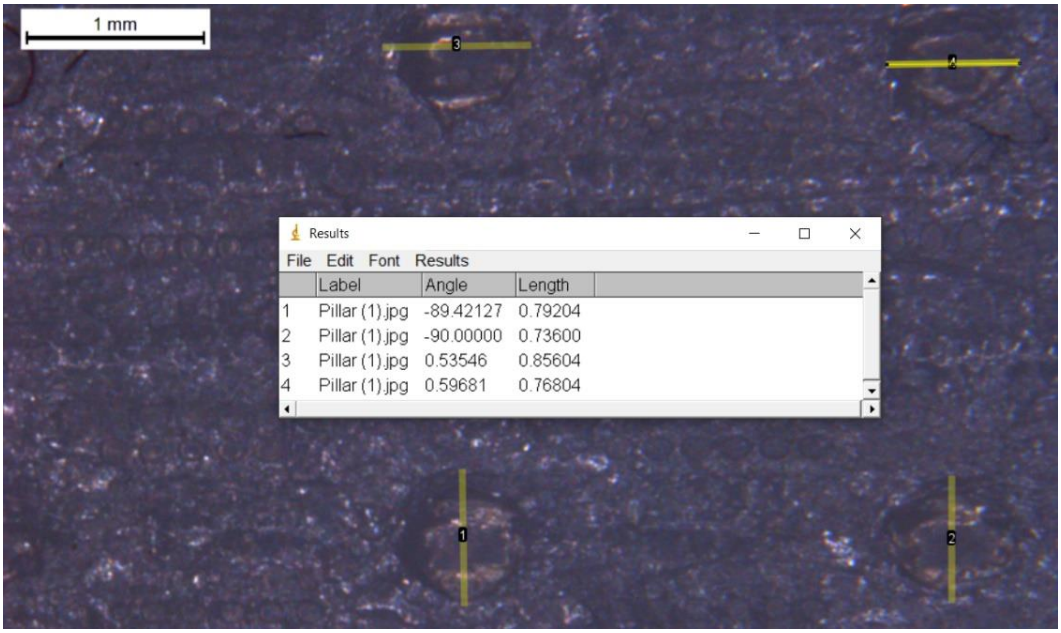

Fig. 3.9 – Samples of Pillar length and width for the Matte device taken at optical microscope.

The device section was observed at the optical microscope for verify that the partitioning bars and the electrode channels were fabricated (see Fig. 3.10).

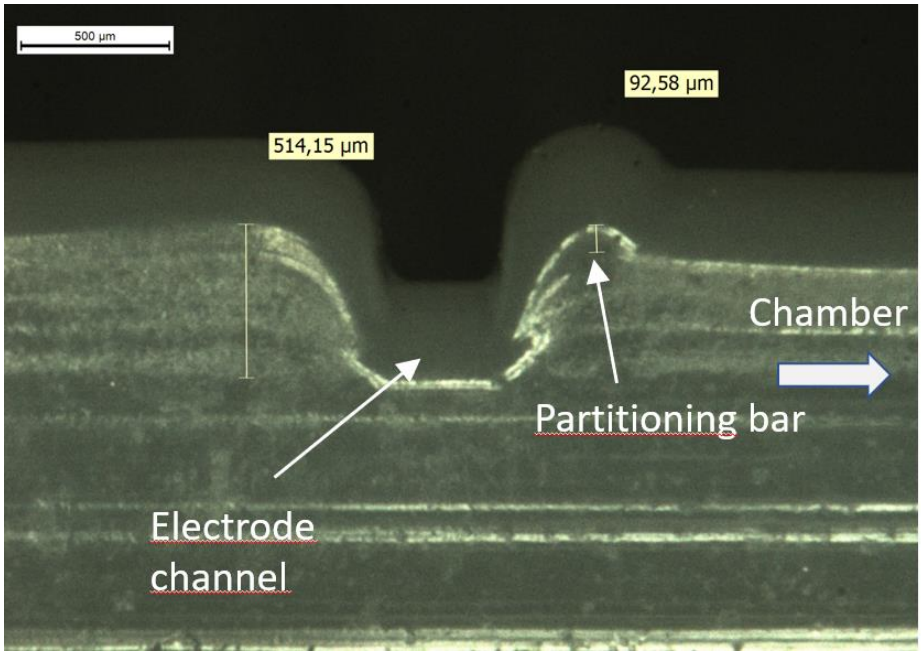

Fig. 3.10 – The section of the µFFE device at optical microscope for the prototype with 70 µm high partitioning bars.

3.3 Inlets/outlets and electrodes results

The printing mode performance comparison was realized also for the inlet/outlet diameters and for the electrode width to determine the more accurate one. Measurements were realized at optical microscope for four Glossy finish and one Matte finish devices. Concerning the glossy surface finished, eleven samples for circle diameter (see Fig. 3.13 and Fig. 3.14) were acquired for each device and eleven samples for the electrode channels width (see Fig. 3.11 and Fig. 3.12) were acquired. On the Matte device only two sample for the diameter and eleven sample for the electrode channel width were acquired. The results in terms of average value and error (standard deviation of the mean) are reported in table 3.6.

Features	Dimension	CAD (μm)	Glossy actual (μm)	Matte actual (μm)
Inlet/outlet	Diameter	2690	2813 ± 42	2513 ± 95
Electrode channel	Width	500	607 ± 6	415 ± 18

Tab. 3.5 – Inlet/Outlet and electrode for Glossy and Matte devices (average and standard deviation values).

The printing accuracy for the inlet/outlet diameter is around 4.6 % for the glossy surface finished and 6.6% for the Matte one. In this last case, the standard deviation is higher. The printing accuracy for the electrode channels is around 21% for the Glossy surface finished and 15% for the Matte one (see Tab. 3.5).

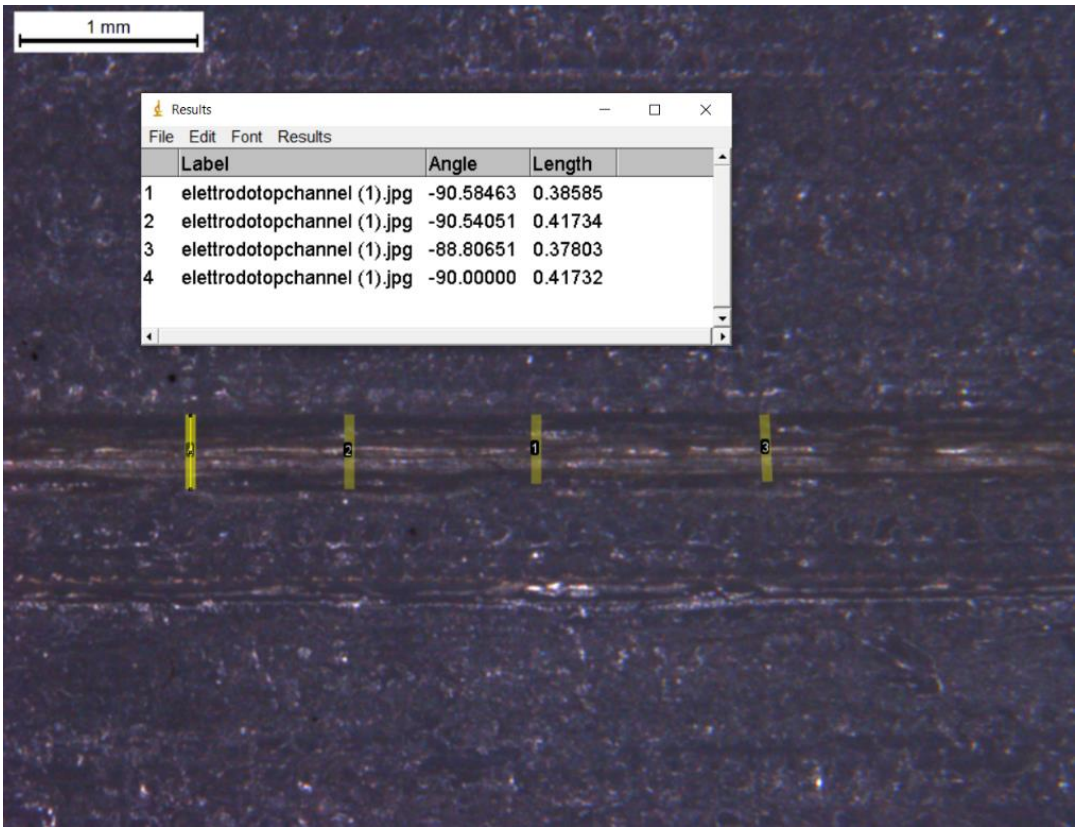

Fig. 3.11 – Samples of electrode width for a Matte fabricated device taken at the optical microscope.

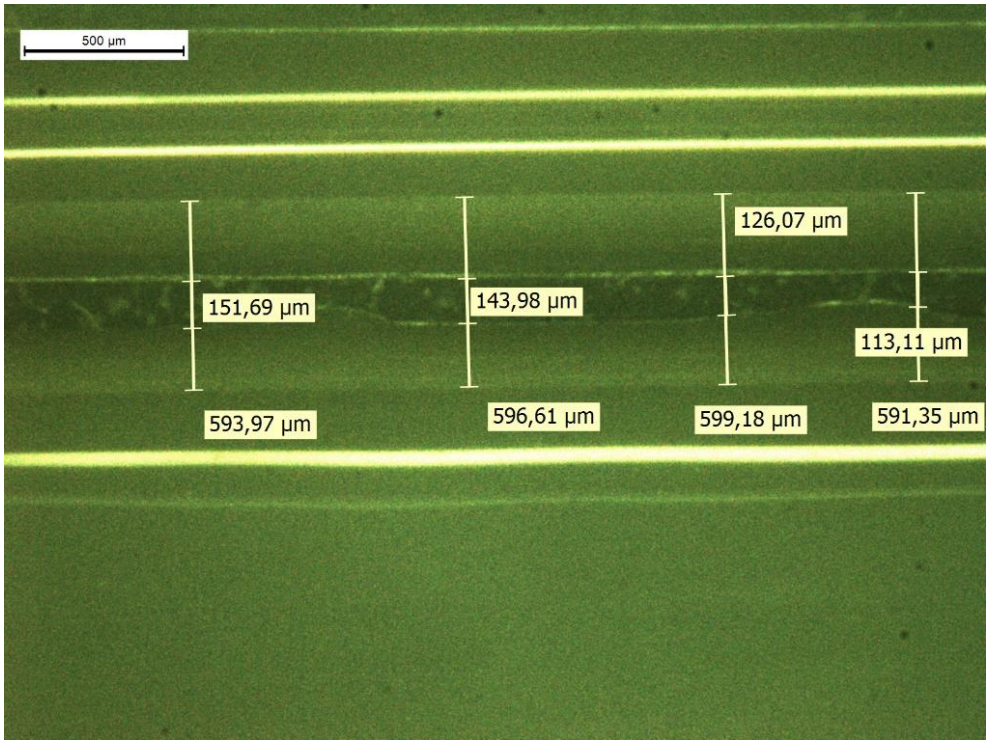

Fig. 3.12 – Samples of electrode width for the Glossy device taken at the optical microscope.

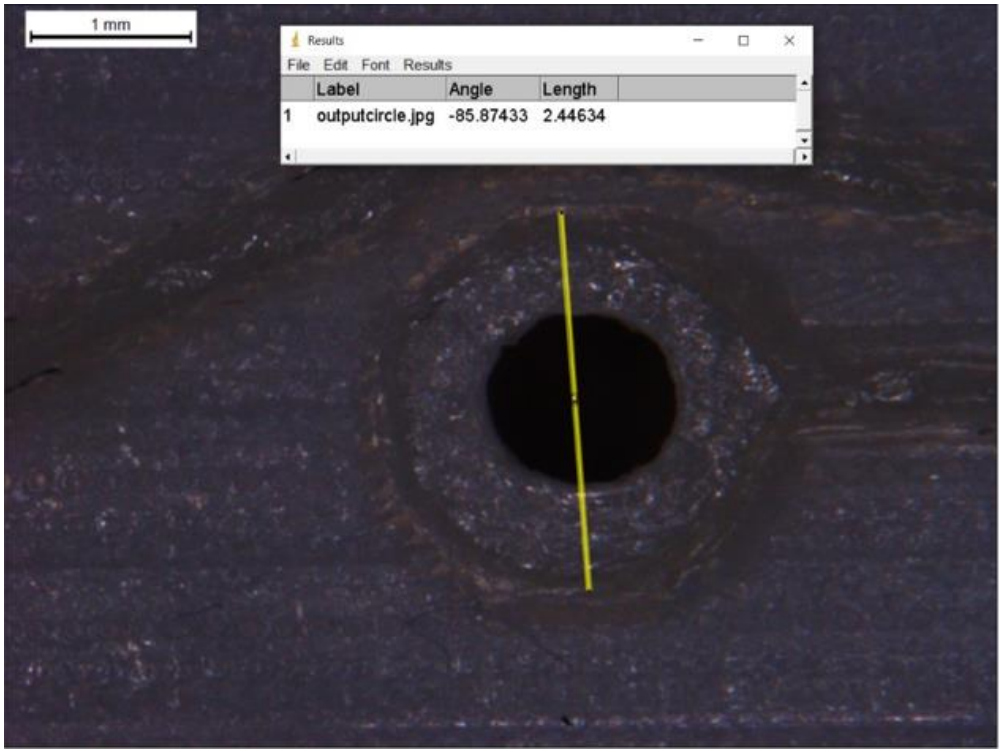

Fig. 3.13 – Measurements of inlet/outlet diameter for a Matte fabricated device realized at the optical microscope.

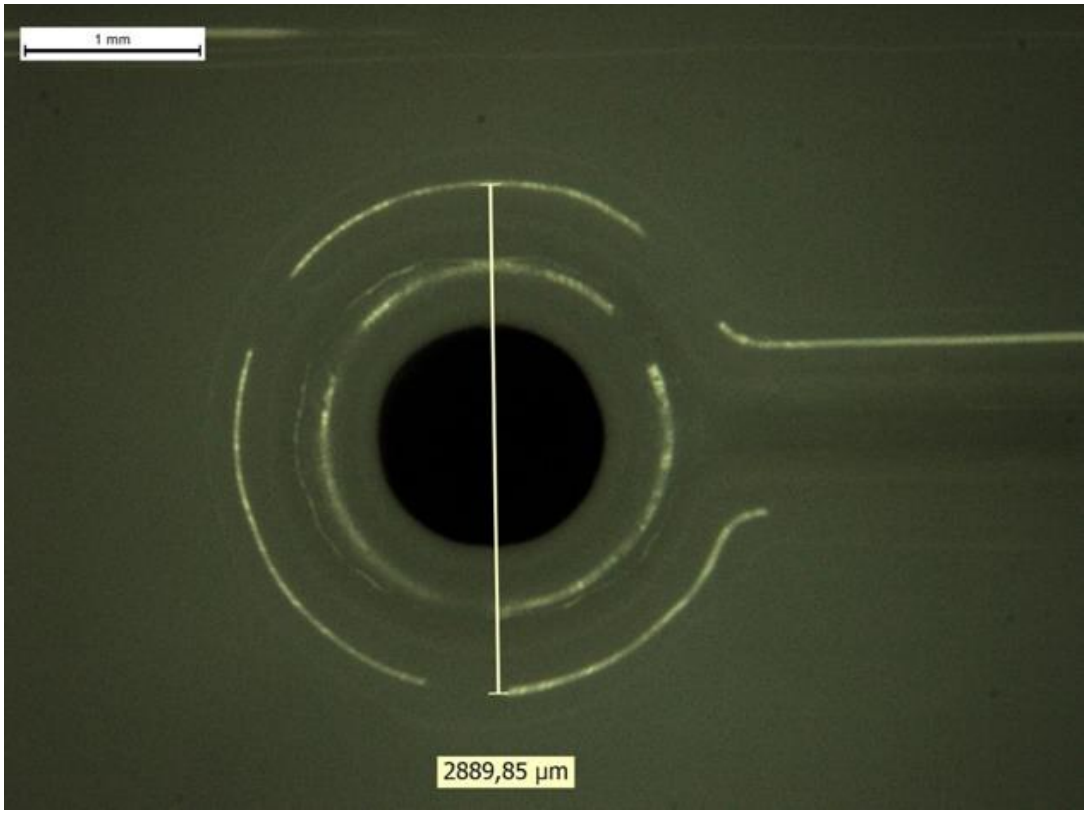

Fig. 3.14 – Measurements of inlet/outlet diameter for a Glossy device realized at the optical microscope.

.

3.4 Surface roughness

During the device fabrication, the surfaces were not fabricated perfectly smooth by the machine. The separation chamber floor is full of micro-defects which are introduced during the building process. The roughness is the physical property that quantifies such imperfections. The surfaces imperfections reduce the optical efficiency of the devices and create some surface dependent phenomena which distort the flows profile and create localized pressure differences. In this section, measurements of roughness were realized in different points of the separation chamber floor by using the profilometer (see Fig. 3.15 and Fig. 3.16). In particular ten samples for two Glossy surface finished devices and ten samples for one Matte surface finished device were acquired. The results were mediated to make a comparison (see Tab. 3.6).

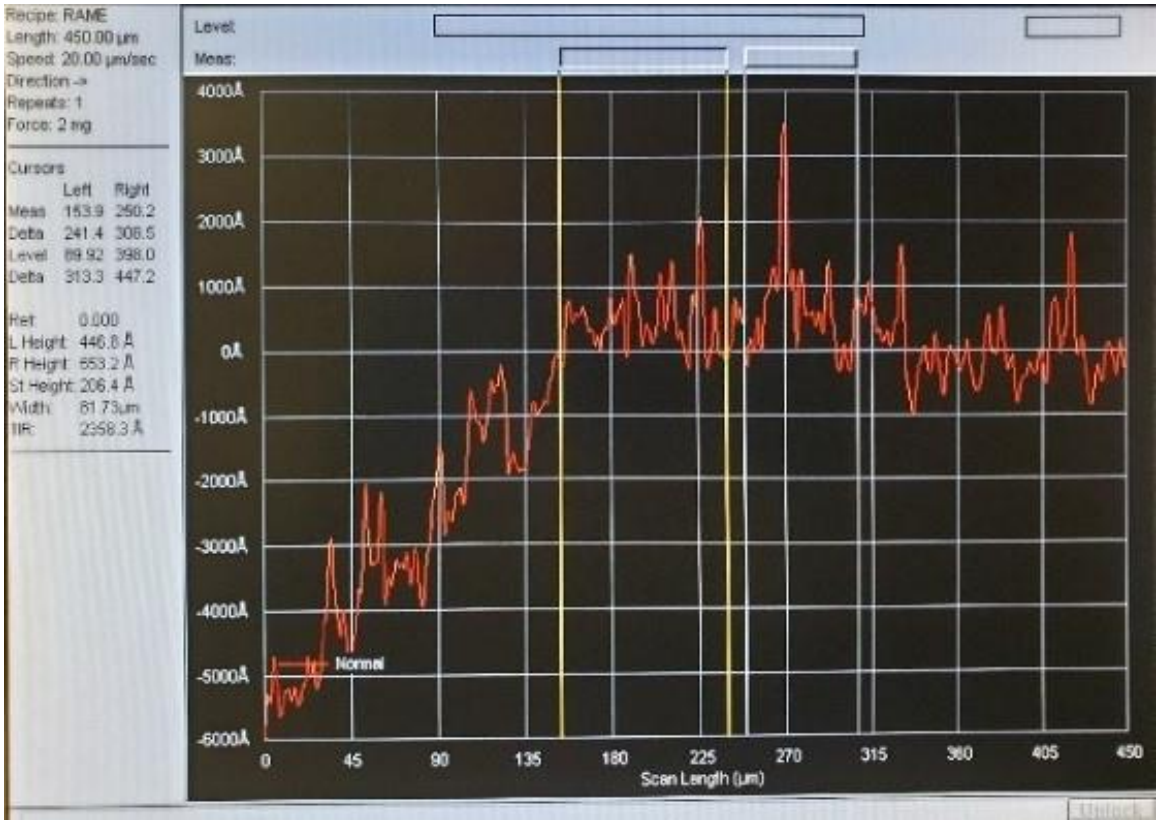

Fig. 3.15 - P10 image of roughness profile acquisition for a Glossy surface finished.

Surface finished	**Roughness (nm)**
Glossy	50 ± 26
Matte	410 ± 100

Tab. 3.6 – Roughness results (average and standard deviation values).

The average value obtained for the glossy mode is in the order of tens of nanometer. This mode is better from the roughness with respect to the Matte one in which the value is one order of magnitude larger and lead therefore to higher reproducibility variance. For such a reason, the Glossy surface finished is the better one.

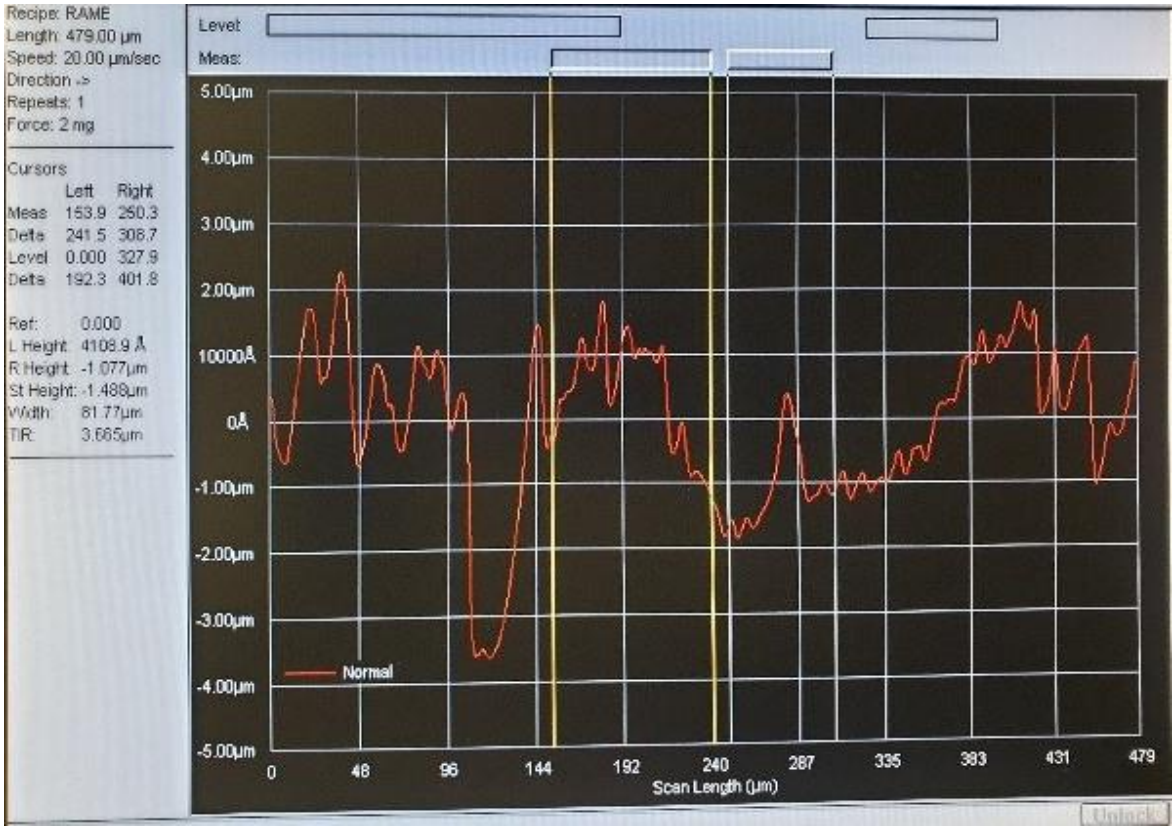

Fig. 3.16 - P10 image of roughness profile acquisition for a Matte surface finished fabricated device.

4.

Separation tests

In this section the results of separation tests carried out with one of the fabricated μFFE devices are illustrated. In particular after having tested the correct bonding of the chamber through the performance of leakage tests, the electrophoresis has been performed with the aim of separating a mix Bromophenol Blue (2,6-dibromo-4-[3-(3,5-dibromo-4-hydroxyphenyl)-1,1-dioxo-2,1λ⁶-benzoxathiol-3-yl]phenol) and Xylene Cyanol FF (1,3-Benzenedisulfonic acid, 4-[[4-(ethylamino)-3-methylphenyl][4-(ethylimino)-3-methyl-2,5-cyclohexadien-1-ylidene]methyl]-, sodium salt (1:1)), which are two dyes commonly employed in the electrophoresis processes.

4.1 Experiments setup

In this section, the experiments setup is described. All the tests were realized in a workplace suitable to conduct microfluidic experiments. In particular, it was provided by all the required equipment. During this phase, the fabricated Lab-On-A-Chip is connected to a fluidic net which has as a main core a pumping system (HARVARD APPARATUS Pump33, Hollinston, MA, USA). This system is able to support two syringes having a volume up to 60 mL. To carry out these experiments, two glass syringes which have 250 μL of volume and 2.303 mm of diameter

model 1725 TLL provided by Hamilton were used. This kind of glass syringe is very precise and it allows to dispense the fluids with an accuracy of 1% with the possibility to set the flow rate to a value ranging from a minimum of 0.345 μL/hr to a maximum of 45.18 mL/hr. In particular, they are employed to pump the sample and the buffer solutions inside the microfluidic chamber. The syringes are loaded with the solutions which must be pumped inside the chamber and then firmly anchored to the supports of the pump system to avoid error during the work.

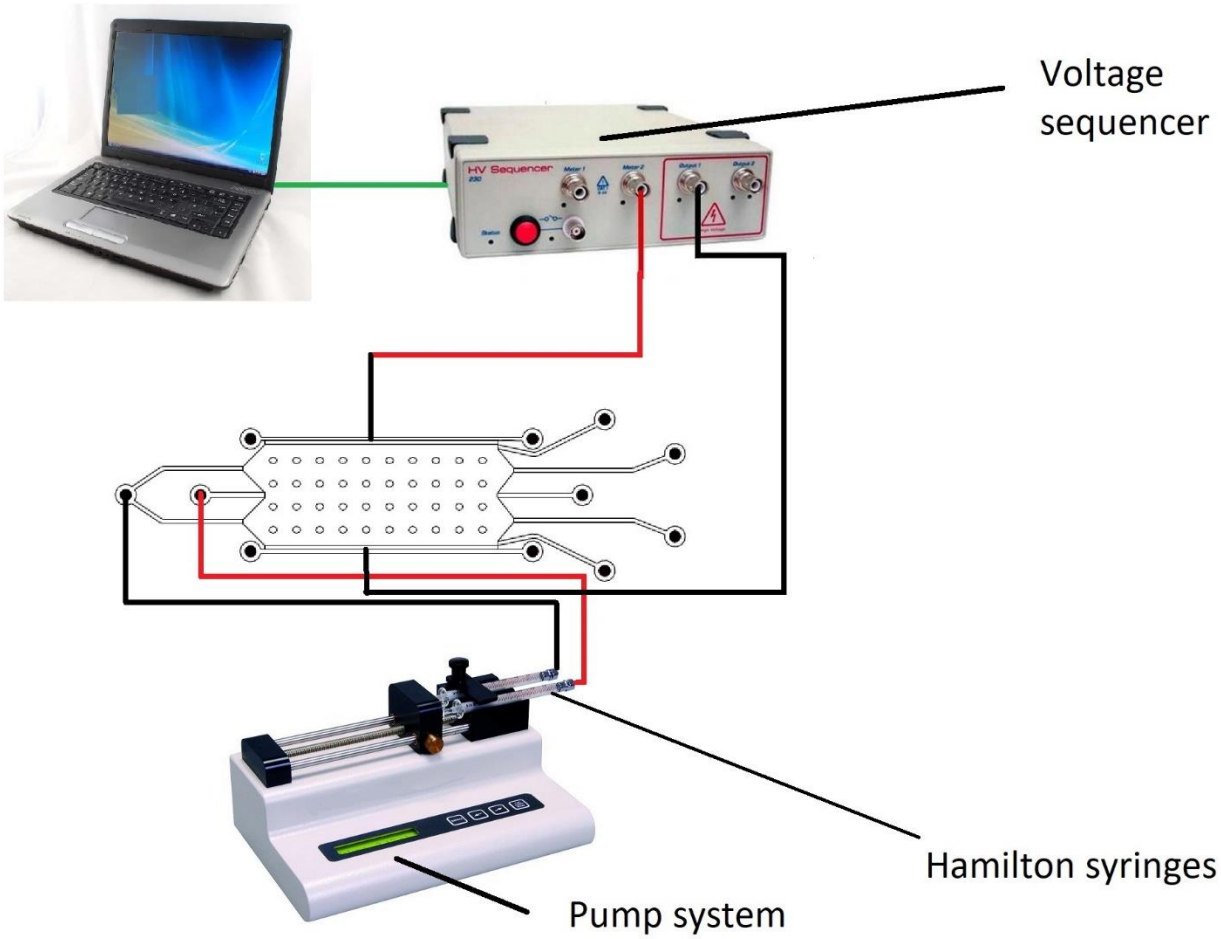

Fig. 4.1 - The voltage sequencer and the pumping system connected to the μFFE device.

The flow rates in the pumping system are set by using the keypad in the front of the system.

4.1.1 Electrical response of the system

Before performing the electrophoresis process, the voltage power supply was connected to the device electrodes. In particular, it was important to assure to provide the correct application of a continuous electric field to the separation chamber.

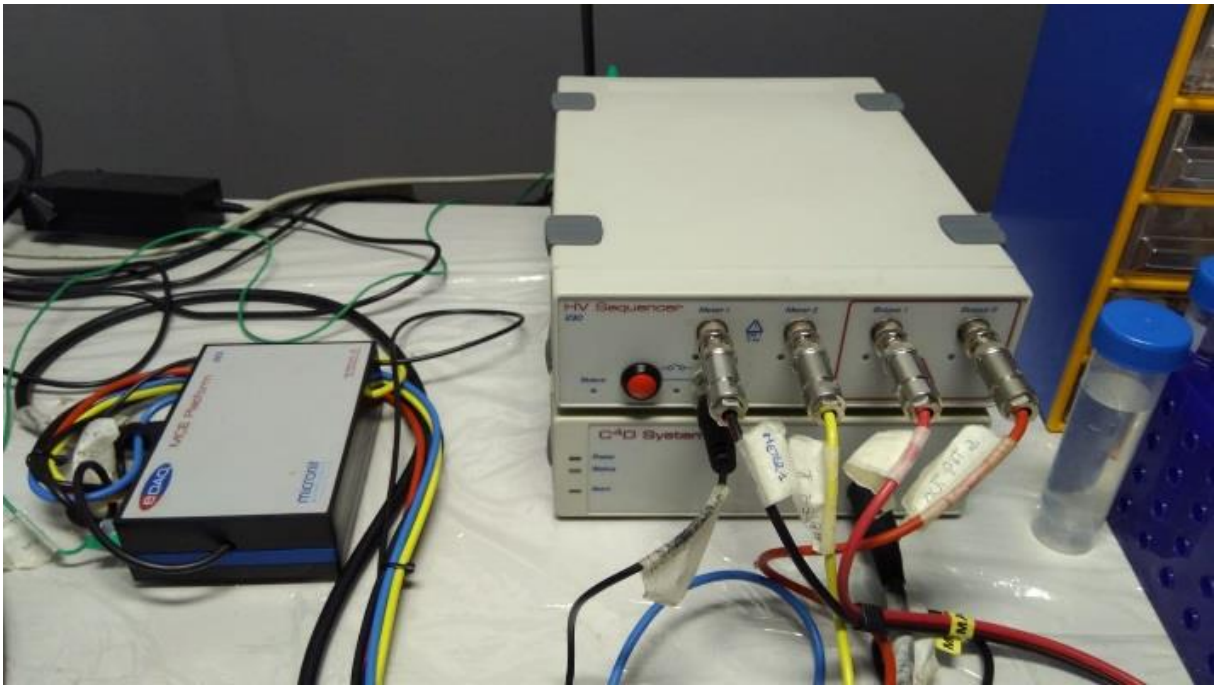

Fig. 4.2 - The voltage sequencer employed to apply the electric field to the separation chamber.

In the free flow electrophoresis, the applied electric field direction is oriented across to the separation chamber perpendicularly. The electric field was applied by means of a voltage sequencer generator (CD HV 230 Sequencer, Marciana, Italy) provided by its own custom software through which it was possible to set the applied voltage and the application field time. Focusing on the electrical connections, the chip electrode wires were wrapped around a galvanized screw. Then, the anchorage to the electrical equipment was made by clamping the generator cables to the

device by means of crocodile clips. Then, voltages have been applied to the system and the corresponding values were measured at the terminals of the cable by measuring with a digital multimeter in order to quantify the voltage drop introduced by the connection.

4.2 Leakage tests

In this phase, the sealed chips obtained after the bonding procedure were tested to assure the strength of the PMMA-VeroWhitePlus (RGD835) bonding. In particular, to carry on this simple test, a colored solution properly diluted was employed to check if fluid leaks were coming from the microfluidic chamber. The devices were filled with a orange common food dye to test the strength and uniformity of the bonding procedure. Initially, the results were not good because of the little manual experience in spreading the resin which leads to void creations. However, by applying several times the bonding technique, a quite uniform sealing was obtained. The dye solution was pumped inside the microfluidic chamber at different flow rates in order to test the bonding strength. Initially, the flow rate was set to 5 μL/min in order to test if there were significant errors committed during the bonding procedure. Subsequently, the velocity was increased until 60 μL/min which was the maximum flow rate sustained by the device. For flow rates higher than this limit, the bonding started to give away and the fluid exited the chamber. Concerning the standard connectors, the device with 18.70 mm Luer slip connectors guaranteed a strong anchoring to the net pipes. Indeed, not significant fluid quantity came out. Subsequently, other quality tests were performed by connecting the device with 2.90 mm Luer slip connectors. In this case, there were evident connection problems. The chamber was filled faster thanks to the reduced dead volume, but losses were noticed. Indeed, after a small amount of time, the chamber starts to fill with air bubbles. Finally, quality tests were performed for the device that mounts the threaded UNF 28 standard connectors. Finally, it is the best kind of fabricated connector. Indeed, no leakages were observed. The sample and buffer pipes were firmly connected to the device and the fluids were pumped without pressure losses.

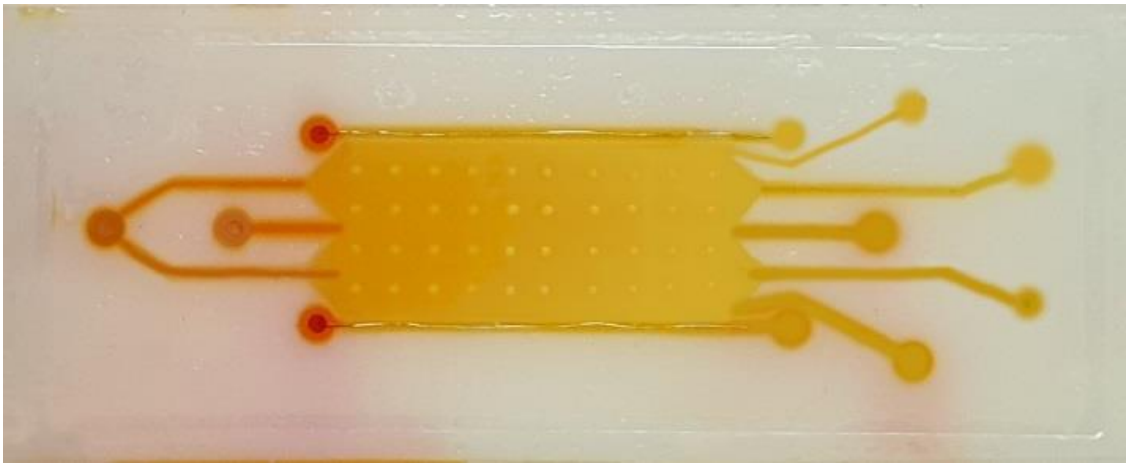

Fig. 4.3 - The sealed chamber filled with a common orange food dye.

4.3 Device preparation

After testing the electrical connections, the separation chamber of the device has been filled in order to be cleaned with proper solutions. Initially, the water has been pumped inside the device with the aim of flushing out dust particles which accidentally entered inside the microfluidic channels during the bonding procedure. Subsequently, a solution of Ethanol 70% (w/w) (purchased from Sigma-Aldrich) has been used to clean the separation chamber and the syringes finely. If another cleaning phase was required after the realization of a separation test, attention has been spent to respect the order of the employed solutions exactly in order to avoid surface adsorption problems with the analytes. After each experiment, the glass syringes, the tubes and the connectors have been intensively cleaned with the same procedure used before being employed for a new one.

4.4 Buffer solution preparation

The employed buffer to carry on the separation tests was a 20mM (pH 7) HEPES (N-2-Hydroxyethylpiperazine-N'-2-Ethanesulfonic acid) solution. It is pumped through a special inlet which is located behind the sample one (see Fig. 2.3). The buffer flow has the function to confine well the electrophoretic separation process by reducing in such way the flow sample stream broadening a non ideality which reduces the separation resolution. Moreover, the buffer solution is bio-compatible and it suits well to perform the electrophoresis of biological samples. It is prepared by diluting 0,2383 gr of HEPES salts into 50 mL of bi-distillated water, knowing that the molar mass is equal to 238,3012 g/mol.

.4.5 Dyes mixture separation

In this section, separation tests were performed by using the fabricated μFFE device. The main objective was to find the best voltage and flow rate combination to obtain the best separation as possible of a dye mixture composed by Bromophenol Blue and Xylene Cyanol FF two dyes commonly employed in the electrophoresis processes [49]. In this phase, the separation chamber of the cleaned chip was filled with the buffer solution completely. The two glass syringes were filled, attached to the pumping system and connected to the sample and buffer inlets. At this point, a flow rate around 30 μL/min was set on the pump system for both channels in order to fill the chamber volume with the buffer solution quickly. Before having started the tests, the dye mixture was closed in an Eppendorf and it was immersed in an ultrasonic bath for 20 minutes. This step is fundamental since this process mixes the sample solution uniformly and it removes dissolved gas from liquid. The sample was loaded inside the separation chamber. As already mentioned, the buffer flow acts to confine the electrophoresis separation process and to avoid diffusion phenomena (see Fig. 4.4).

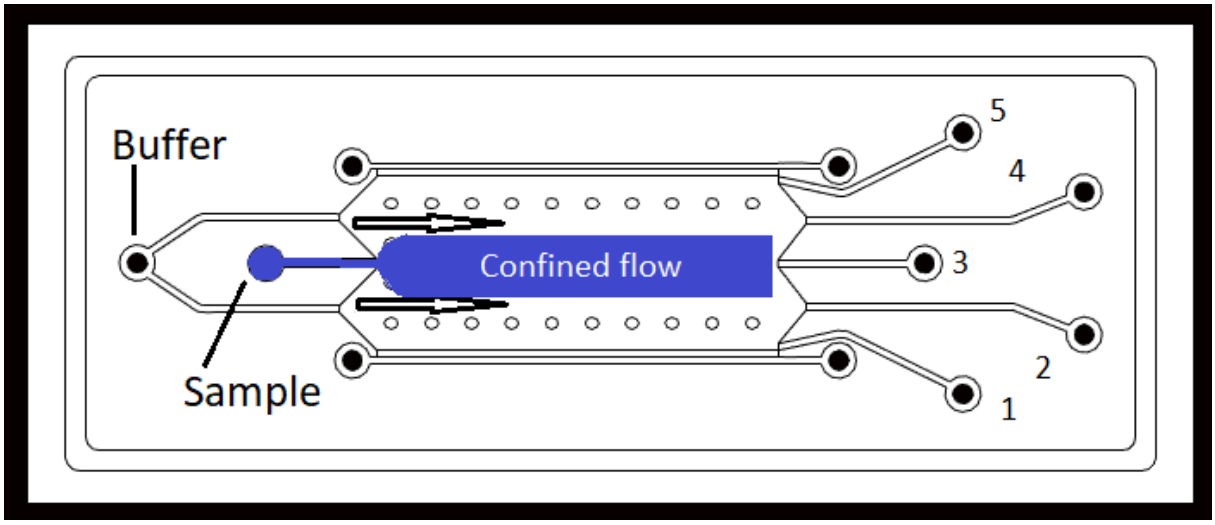

Fig. 4.4 - The flow confinement inside the separation chamber due to the buffer flow.

The test performed are resumed in the Tab. 4.1.

Separation Test	Duration test (s)	Nominal voltage (V)	Measured voltage (V)	Sample flow rate (µL/min)	Buffer flow rate (µL/min)
1)	300	150	123.8	15	15
2)	300	150	123.8	10	10
3)	300	150	123.0	5	5
4)	300	150	123.0	1	1
5)	300	120	97.3	15	15
6)	300	120	97.3	10	10
7)	300	120	98.9	5	5
8)	300	120	99.0	1	1

Tab. 4.1 - Separation tests.

The tests were performed by changing the flow rate each time by maintaining the voltage fixed. The values shown on Tab. 4.1 were chosen on the basis of preliminary separation tests. The buffer and the sample flow rate ratio was kept 1:1 during the experiments. The electrophoresis process was observed in different times (see Fig. 4.5).

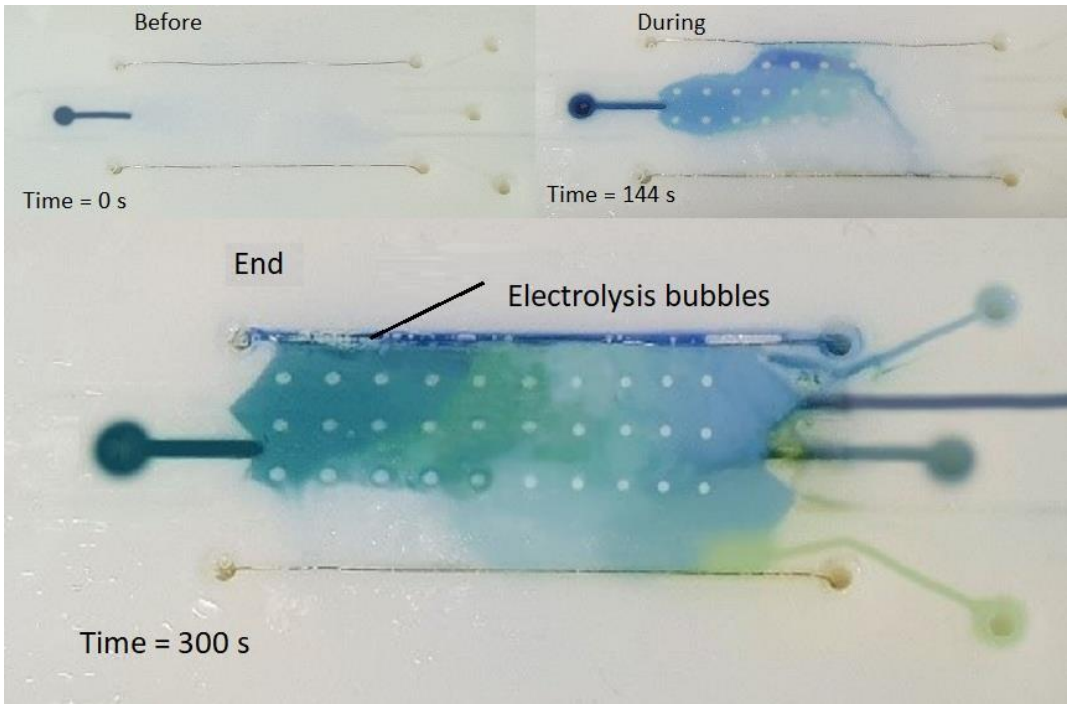

Fig. 4.5 - Temporal sequence of the separation tests.

Consideration concerning the tests performed are reported on Tab. 4.2.

Separation Test	**Report**
1)	For such parameters, the buffer flow did not confine the separation process. After about two minutes, the xylene cyanol FF started to migrate towards the lower electrode.
2)	After about two minutes of the electric field application, the Xylene Cyanol can be seen. A clear separation was observed after four minutes.
3)	Like in the previous test, the separation was barely visible but the process was confined in a narrow space.
4)	In this test, the separation was barely visible and there was a principle of flow confinement.
5)	After about 3 minutes, the separation was clearly visible.
6)	The separation was visible at the end of the test.
7)	The separation was not visible.
8)	At the end of the test, a separation was visible.

Tab. 4.2 - Separation test reports

The first four tests were realized for a voltage value equal to 150 V, the flow confinement was better in the case of flow rates equal to 1 μL/min and 5 μL/min with respect to 10 μL/min and 15 μL/min since in these last two cases, the confinement was practically not observed (see Fig. 4.7). Moreover, the best electrophoresis result was obtained to 15 μL/min of flow rate. Subsequently, the voltage was set to 120 V in order to observe improvements in the separation. In this case, the flow rate was changed four times (see Fig. 4.8). The best result for the flow confinement was obtained again for 1 μL/min and 5 μL/min flow rate. The best result in terms of separation visibility was obtained for 15 μL/min. To summarize, the more significant separation was obtained in the case of the voltage equal to 150 V and of flow rates equal to 10 μL/min since in this case, after the electrophoresis process, the dye separation was clearly visible.

The best confinement was obtained for the voltage equal to 120V and flow rates equal to 1 μL/min. In particular, by decreasing the flow rate and by keeping fixed the applied voltage, the separation was better confined.

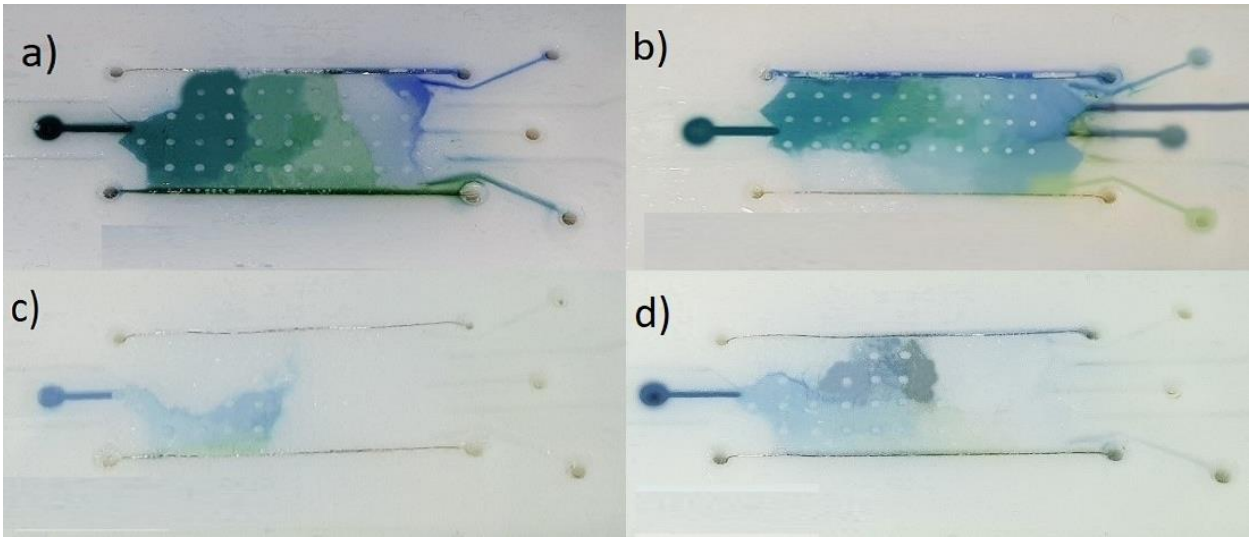

Fig. 4.6 – The voltage is set equal to 150V, (a) Test for 15 μL/min, (b) Test for 10 μL/min, (c) Test for 5 μL/min, (d) Test for 1 μL/min.

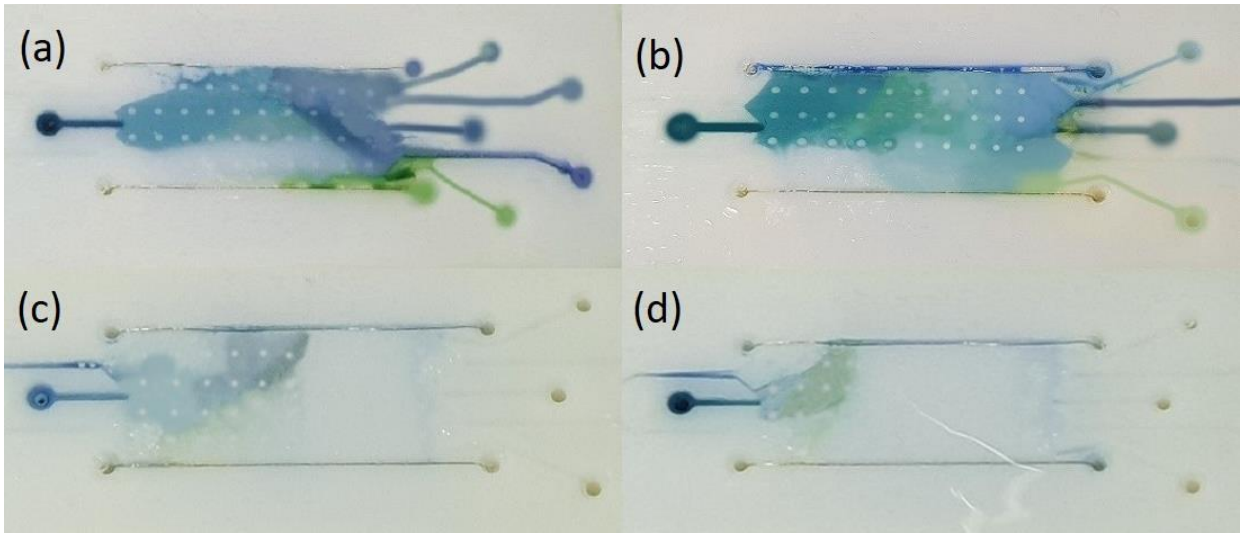

Fig. 4.7 – The voltage is set equal to 120V, (a) Test for 15 μL/min, (b) Test for 10 μL/min, (c) Test for 5 μL/min, (d) Test for 1 μL/min.

5.

Conclusions and future works

Concerning the performances of the Glossy and Matte fabrication modes, the first one is in general more accurate. In particular, the best printing accuracy is obtained for the Pillar height with a discrepancy with respect to the CAD value equal to 0.4 %. On the contrary, the accuracy results obtained for the Matte surface finished are not acceptable and they are worse in fabricating all device features. In particular, the worst fabrication results of this surface finished are obtained for pillar length and width with accuracy values equal to 18% and 20%. Concerning the electrode fabrication, the results provided by the OBJET 30 in fabricating such features are bad for both surfaces finished. The presence of the partitioning bars, close to such channels, provides problems. Therefore, future improvements in the design are needed to solve this problem. Focusing on the glossy mode, the width increment of the partitioning bars from 500 μm to 800 μm leads to an important accuracy reduction by passing from 3.4% to 9.75 %. Concerning the surface roughness, the Glossy surface finished is surely better with respect to the Matte one since there is an order of magnitude by passing from 50 nm for the first case to 410 nm for the second one. In the second case, the results show a greater reproducibility variance.

By summarizing, the best mode in terms of fabrication accuracy and roughness to manufacture this master thesis μFFE device is the Glossy one. However, deeper analysis should be performed

by increasing the number of measurements and by providing further design modifications.

Focusing on the Bromophenol Blue and Xylene Cyanol FF dye mixture separation, the best parameters configuration for a clear dye electrophoretic separation is 150 V of voltage and 10 μL/min of flow rates. The best case for the flow confinement inside the separation chamber is obtained when the voltage is equal to 120 V and the flow rates are equal to 1 μL/min. Moreover, fixed the applied voltage, the flow confinement decreases with the increasing of the flow rates.

In conclusion, a μFFE device has been successfully designed, fabricated and tested. 3D printing has been found to be a versatile technique to rapidly pass from the microfluidics design to a functional prototype fabrication, thus obtaining advantages in terms of time and cost. Separation experiments were also successfully conducted thus giving a very preliminary indications for the next bio experiments implementation.

6. Appendix

6.1 Summary

This master's degree thesis focuses on developing a microfluidic Lab-On-A-Chip that implements the micro free-flow electrophoresis (μFFE) for the exosome lung cancer's biomarkers detection. The realized device is a novelty in the state of the art and it is proposed to replace the standard slower separation techniques commonly employed for the exosomes isolation such as centrifugation and chromatography etc. The exosomes are nanosized vesicles containing DNA, mRNA and proteins which are released in the extracellular environment and are fundamental to understand the cellular communication. The profiling of proteins contained by these nano-sized vesicles could help in speed up the NSLC (Non-Small cell Lung Cancer) diagnosis. Therefore, the device proposed in this thesis manages to perform an efficient molecular separation by exploiting the electrophoresis technique. In this chip, the analytes of interest are isolated by applying an electric field in the direction perpendicular with respect to a sample flow inside a separation chamber. In particular, after a certain amount of time under the force of the electric field, the molecules or particles start to migrate in the lateral direction according to their size and electric charge. Then, they are collected at the output section of the device.

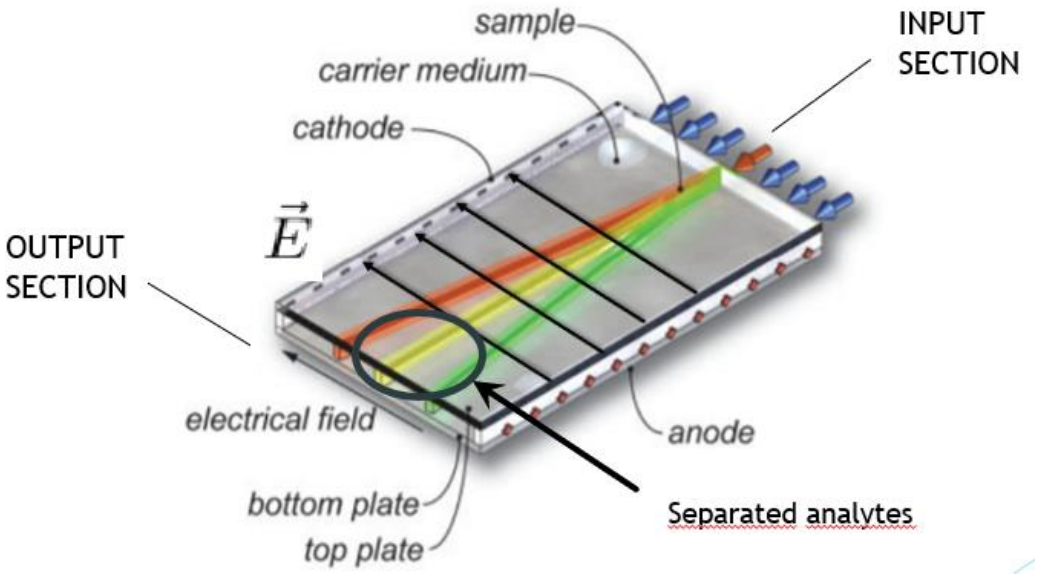

Fig. 6.1 – The picture shows a μFFE device in function. The analytes are collected at the output section after a certain amount of time under the force of the electric field.

The chip proposed in this work has been designed by using a commercial computer graphic CAD software called Rhinoceros and it has been fabricated by employing the 3D printing technique. In particular, the 3D printer mod. OBJET 30 manufactured by Stratasys has been employed for the fabrication. This machine is based on an efficient technology which is called PolyJet. The chapter one describes in general the electrophoresis technique and in detail the free flow zone one. Moreover, the state of the art of the existing micro free-flow electrophoresis devices, their main applications, their main fabrication techniques and their materials are investigated. The chapter two describes in detail the design of the chip, the geometry and all the device features. Moreover, the 3D printing fabrication technique is introduced and the PolyJet fabrication technology is described. Very important in this chapter, is the definition of two fabrication modes proper of the 3D printing technique, the Glossy and the Matte. They have been employed during the work to fabricate devices with different surface finished. The main objective of this work has been to compare the OBJET 30 performances in fabricating μFFE chips in Glossy and Matte and in particular to determine if the first mode was better in terms of accuracy and roughness with respect to the second one for the reproducibility of the 3D printing process. The chapter three contains the fabrication results and their discussion. In particular, the dimensions

of the built prototypes are compared with the nominal reference values which have been set on the CAD with the aim to determine for which fabrication mode the manufacturing was more accurate. After the device fabrication, the quality of the chip sealing was investigated and separation tests were performed. Then, another objective has been to determine which were the best separation parameters in terms of voltage, buffer and sample flow rate to obtain the best process confinement and the best visible separation in the case of the electrophoresis of a mixture composed by Bromophenol Blue and Xylene Cyanol FF, two dyes commonly employed in the electrophoresis processes. The chapter four describes the experiment setup and contains the separation test results with their discussion. The chapter five contains the conclusions. Concerning the fabrication performances of the Glossy and Matte fabrication modes, the first one was more accurate and therefore it is better for the reproducibility of this Lab-On-A-Chip. Concerning the separation tests, the best parameters configuration for a clear dye electrophoretic separation was 150 V of voltage and 10 μL/min of flow rates. The best case for the separation process confinement was obtained when the voltage was equal to 120 V and the flow rates were equal to 1 μL/min. In conclusion, a μFFE device has been successfully designed, fabricated and tested. 3D printing has been found to be a versatile technique to rapidly pass from the microfluidics design to a functional prototype fabrication, thus obtaining advantages in terms of time and cost. Separation experiments were also successfully conducted thus giving a very preliminary indications for the next bio experiments implementation.

References

[1] Strimbu, K., & Tavel, J. A. (2010). What are biomarkers? Current Opinion in HIV and AIDS, 5(6), 463–466.

[2] Zheng, H., Zhan, Y., Liu, S., Lu, J., Luo, J., Feng, J., & Fan, S. (2018). The roles of tumor-derived exosomes in non-small cell lung cancer and their clinical implications. Journal of Experimental & Clinical Cancer Research, 37(1).

[3] Yu, L.-L., Zhu, J., Liu, J.-X., Jiang, F., Ni, W.-K., Qu, L.-S., Ni, R.-Z., Lu, C.-H., & Xiao, M.-B. (2018). A Comparison of Traditional and Novel Methods for the Separation of Exosomes from Human Samples. BioMed Research International, 2018, 1–9.

[4] Ou, X., Chen, P., Huang, X., Li, S., & Liu, B. (2019). Microfluidic chip electrophoresis for biochemical analysis. Journal of Separation Science, 43(1), 258–270.

[5] Zhang, C.-X., & Manz, A. (2003). High-Speed Free-Flow Electrophoresis on Chip. Analytical Chemistry, 75(21), 5759–5766.

[6] Turgeon, R. T., & Bowser, M. T. (2009). Micro free-flow electrophoresis: theory and applications. Analytical and Bioanalytical Chemistry, 394(1), 187–198.

[7] Raymond., De et al. (1995). Continuous Sample Preparation Using Free-flow electrophoresis On A Silicon Microstructure. Proceedings of the International Solid-State Sensors and Actuators Conference - TRANSDUCERS '95 1: 760-763.

[8] Kostal, V., Fonslow, B. R., Arriaga, E. A., & Bowser, M. T. (2009). Fast Determination of Mitchondria Electrophoretic Mobility Using Micro Free-Flow Electrophoresis. Analytical Chemistry, 81(22), 9267–9273.

[9] Jender, Matthias; Novo, Pedro; Maehler, Dominic; Münchberg, Ute; Janasek, Dirk; Freier, Erik (2020): Multiplexed Online-Monitoring of Microfluidic Free-Flow Electrophoresis via Mass Spectrometry. ChemRxiv. Preprint.

[10] Sun, W.-W., Dai, R.-J., Li, Y.-R., Dai, G.-X., Liu, X.-J., Li, B., Lv, X., Deng, Y.-L., & Luo, A.-Q. (2020). Separation of proteins and DNA by microstructure-changed microfuidic free flow electrophoresis chips. Acta Astronautica, 166, 573–578.

[11] Jing, M., & Bowser, M. T. (2011). Isolation of DNA aptamers using micro free flow electrophoresis. Lab on a Chip, 11(21), 3703.

[12] Todaro, C. M. (2014). Centrifugation. In Fermentation and Biochemical Engineering Handbook (pp. 267–281).

[13] Hügle, M., Dame, G., Behrmann, O., Rietzel, R., Karthe, D., Hufert, F. T., & Urban, G. A. (2018). A lab-on-a-chip for preconcentration of bacteria and nucleic acid extraction. RSC Advances, 8(36), 20124–20130.

[14] Kohlheyer, D., Eijkel, J. C. T., Schlautmann, S., van den Berg, A., & Schasfoort, R. B. M. (2008). Bubble-Free Operation of a Microfluidic Free-Flow Electrophoresis Chip with Integrated Pt Electrodes. Analytical Chemistry, 80(11), 4111–4118.

[15] Yazdi, M. K., Vatanpour, V., Taghizadeh, A., Taghizadeh, M., Ganjali, M. R., Munir, M. T., … Ghaedi, M. (2020). Hydrogel membranes: A review. Materials Science and Engineering: C, 114, 111023.

[16] Takehara, H., Sato, S., & Ichiki, T. (2019). All-polymer-based micro free-flow electrophoresis (μFFE) device with cellulose permeable membranes. Applied Physics Express, 12(10), 107001.

[17] Rudisch, B. M., Pfeiffer, S. A., Geissler, D., Speckmeier, E., Robitzki, A. A., Zeitler, K., & Belder, D. (2019). Nonaqueous Micro Free-Flow Electrophoresis for Continuous Separation of Reaction Mixtures in Organic Media. Analytical Chemistry.

[18] Pfeiffer, S. A., Rudisch, B. M., Glaeser, P., Spanka, M., Nitschke, F., Robitzki, A. A., Schneider, C., Nagl, S., & Belder, D. (2017). Continuous purification of reaction products by micro free-flow electrophoresis enabled by large area deep-UV fluorescence imaging. Analytical and Bioanalytical Chemistry, 410(3), 853–862.

[19] Köhler, S., Weilbeer, C., Howitz, S., Becker, H., Beushausen, V., & Belder, D. (2011). PDMS free-flow electrophoresis chips with integrated partitioning bars for bubble segregation. Lab Chip, 11(2), 309–314.

[20] Raymond, D. E., Manz, A., & Widmer, H. M. (1994). Continuous Sample Pretreatment Using a Free-Flow Electrophoresis Device Integrated onto a Silicon Chip. Analytical Chemistry, 66(18), 2858–2865.

[21] Bustillo, J. M., Howe, R. T., & Muller, R. S. (1998). Surface micromachining for microelectromechanical systems. Proceedings of the IEEE, 86(8), 1552–1574.

[22] Fu, X., Mavrogiannis, N., Ibo, M., Crivellari, F. and Gagnon, Z.R. (2017), Microfluidic free-flow zone electrophoresis and isotachophoresis using carbon black nano-composite PDMS sidewall membranes. ELECTROPHORESIS, 38: 327-334.

[23] Giboz, J., Copponnex, T., & Mélé, P. (2007). Microinjection molding of thermoplastic polymers: a review. Journal of Micromechanics and Microengineering, 17(6), R96–R109.

[24] Attia, U. M., Marson, S., & Alcock, J. R. (2009). Micro-injection moulding of polymer microfluidic devices. Microfluidics and Nanofluidics, 7(1), 1–28.

[25] Berthold, A., Nicola, L., Sarro, P. ., & Vellekoop, M. . (2000). Glass-to-glass anodic bonding with standard IC technology thin films as intermediate layers. Sensors and Actuators A: Physical, 82(1–3), 224–228.

[26] Pan, Y.-J., & Yang, R.-J. (2006). A glass microfluidic chip adhesive bonding method at room temperature. Journal of Micromechanics and Microengineering, 16(12), 2666–2672.

[27] Zhou, W., Xia, L., Xiao, X., Li, G., & Pu, Q. (2019). A microchip device to enhance free flow electrophoresis using controllable pinched sample injections. ELECTROPHORESIS, 40(16–17), 2165–2171.

[28] Libansky, M., Zima, J., Barek, J., Reznickova, A., Svorcik, V., & Dejmkova, H. (2017). Basic electrochemical properties of sputtered gold film electrodes. Electrochimica Acta, 251, 452–460.

[29] Raymond, D. E., Manz, A., & Widmer, H. M. (1996). Continuous Separation of High Molecular Weight Compounds Using a Microliter Volume Free-Flow Electrophoresis Microstructure. Analytical Chemistry, 68(15), 2515–2522.

[30] Ren, K., Zhou, J., & Wu, H. (2013). Materials for Microfluidic Chip Fabrication. Accounts of Chemical Research, 46(11), 2396–2406.

[31] Johnson, A. C., & Bowser, M. T. (2017). High-Speed, Comprehensive, Two Dimensional Separations of Peptides and Small Molecule Biological Amines Using Capillary Electrophoresis Coupled with Micro Free Flow Electrophoresis. Analytical Chemistry, 89(3), 1665–1673.

[32] Victor, A., Ribeiro, J., … F. Araújo, F. (2019). Study of PDMS characterization and its applications in biomedicine: A review. Journal of Mechanical Engineering and Biomechanics, 4(1), 1–9.

[33] Bruijns, B., Veciana, A., Tiggelaar, R., & Gardeniers, H. (2019). Cyclic Olefin Copolymer Microfluidic Devices for Forensic Applications. Biosensors, 9(3), 85.

[34] Collins, Pete. "The Purpose of the Buffer in Electrophoresis" sciencing.com.

[35] FISK, A., & PATHAK, S. (1969). HEPES-buffered Medium for Organ Culture. Nature, 224(5223), 1030–1031.

[36] Essays, UK. (November 2018). Electrophoresis Types and Applications.

[37] Holloway, C. J., & Trautschold, I. (1982). Principles of isotachophoresis. Fresenius' Zeitschrift Für Analytische Chemie, 311(2), 81–93.

[38] Kohlheyer, D., Eijkel, J. C. T., van den Berg, A., & Schasfoort, R. B. M. (2008). Miniaturizing free-flow electrophoresis – a critical review. ELECTROPHORESIS, 29(5), 977–993.

[39] Hofs, B., Brzozowska, A., de Keizer, A., Norde, W., & Cohen Stuart, M. A. (2008). Reduction of protein adsorption to a solid surface by a coating composed of polymeric micelles with a glass-like core. Journal of Colloid and Interface Science, 325(2), 309–315.

[40] Anciaux, S. K., & Bowser, M. T. (2019). Reduced surface adsorption in 3D printed acrylonitrile butadiene styrene micro free-flow electrophoresis devices. ELECTROPHORESIS, 41(3–4), 225–234.

[41] Geiger, M., Harstad, R. K., & Bowser, M. T. (2015). Effect of Surface Adsorption on Temporal and Spatial Broadening in Micro Free Flow Electrophoresis. Analytical Chemistry, 87(23), 11682–11690.

[42] Barbaresco F., M. Cocuzza, F. C. Pirri, S. L. Marasso (2019). A Novel Micro Free-Flow Electrophoresis 3D printed Lab on a Chip for exosomes separation, Micro & Nano Engineering Journal.

[43] Gross, B. C., Erkal, J. L., Lockwood, S. Y., Chen, C., & Spence, D. M. (2014). Evaluation of 3D Printing and Its Potential Impact on Biotechnology and the Chemical Sciences. Analytical Chemistry, 86(7), 3240–3253.

[44] Udroiu, R., & Braga, I. C. (2017). Polyjet technology applications for rapid tooling. MATEC Web of Conferences, 112, 3011.

[45] OBJET 30 materials, https://www.stratasys.com/en/materials/search?technologies=731e07a1a51b42419acd1cb75142dfe6&phrase=Verowhite&sortIndex=0.

[46] Stratasys OBJET 30, https://www.stratasys.com/3d-printers/objet30-prime.

[47] Adhesive Bonding. (2009). In Handbook of Plastics Joining (pp. 145–173). Elsevier.

[48] National Center for Biotechnology Information. PubChem Database. Xylene cyanole FF, CID=23687514, https://pubchem.ncbi.nlm.nih.gov/compound/23687514 (accessed on July 2, 2020).

[49] National Center for Biotechnology Information. PubChem Database. Bromophenol blue, CID=8272, https://pubchem.ncbi.nlm.nih.gov/compound/Bromophenol-blue (accessed on July 2, 2020).

[50] Barbaresco, F., Cocuzza, M., Pirri, C. F., & Marasso, S. L. (2020). Application of a Micro Free-Flow Electrophoresis 3D Printed Lab-on-a-Chip for Micro-Nanoparticles Analysis. Nanomaterials, 10(7), 1277.